J. Fluid Mech. (1989), *vol.* 202, *pp.* 367–402
Printed in Great Britain

The role of transverse secondary instabilities in the evolution of free shear layers

By G. P. KLAASSEN[1] AND W. R. PELTIER[2]

[1] Department of Earth and Atmospheric Science, York University, North York, Ontario, Canada M3J 1P3

[2] Department of Physics, University of Toronto, Toronto, Ontario, Canada M5S 1A7

(Received 9 July 1987 and in revised form 20 October 1988)

Linear stability analyses and nonlinear flow simulations reveal several important features of transverse secondary instabilities of two-dimensional Kelvin–Helmholtz billows and Stuart vortices. Vortex pairing is found to be the most rapidly amplified mode in a continuous spectrum of vortex merging instabilities. In certain not uncommon circumstances it is possible for more than two vortices to amalgamate in a single interaction, demonstrating that the phenomenon that has become known as the pairing resonance in fact has a rather low quality factor. Another form of merging instability in which a vortex is deformed and drained by its neighbours has been revealed by our linear stability analyses of nonlinear shear-layer disturbances. It appears, however, that this vortex draining instability may be important only in unstratified or very weakly stratified flows, since in moderately stratified Kelvin–Helmholtz flow, it is replaced by a highly localized instability which leads to a temporary distortion of the braids. Nonlinear simulations of vortex merging events in moderately stratified, high-Reynolds-number shear layers are compared to the theoretical predictions of our stability analyses. We investigate and quantify the sensitivity of merging events to variations in the initial conditions. The character of the flow after merging instability saturates and the nonlinear aspects of multiple merging events are also considered.

1. Introduction

Numerous laboratory and geophysical observations over the past two decades have established that wave-like trains of two-dimensional vortices known as Kelvin–Helmholtz (KH) billows figure prominently in the evolution of free shear layers possessing a single inflection point in the velocity profile. In many instances, the large-scale structure of these billows is observed to persist even after the introduction of the small-scale disordered motions characteristic of turbulence. At the present time, several distinct secondary flow transitions are known to precede the onset of turbulence in the layer, the details of which depend on the nature of the stratification.

The numerical analyses of Klaassen & Peltier (1985*b*, *c*) established that Kelvin–Helmholtz billows in a shear layer possessing moderate stable stratification can give rise to the spontaneous growth of longitudinal (i.e. spanwise periodic) convective disturbances confined to those regions of the vortex core in which the original stable stratification has been inverted by the roll-up of the billow. This work theoretically validated the physical arguments advanced by Peltier, Hallé & Clark (1978) and Davis & Peltier (1979). The occurrence of this instability was subsequently

confirmed in a new set of tilted-tube experiments (Thorpe 1985) through the streamwise streaks which it engenders on planform shadowgraphs. Three-dimensional organization has also been observed in unstratified shear layers (e.g. Breidenthal 1981; Bernal *et al.* 1980; Jimenez, Cogollos & Bernal 1985; Bernal & Roshko 1986; Lasheras & Choi 1988), although the spanwise wavelengths are much longer than in the inhomogeneous case. Numerical analyses of homogeneous flows by Pierrehumbert & Widnall (1982), Nagata & Busse (1983), and Corcos & Lin (1984) have revealed the existence of a secondary bifurcation which has become known in the literature as 'translative' instability. Both the convective and the unstratified secondary instabilities introduce three-dimensional motions into the shear layer and are thought to be intimately connected with the onset of turbulence.

Another instability in which small-scale wavelike disturbances form on the braids between adjoining billows has been observed by Thorpe (1968) in the laboratory and Woods (1969) in the oceanic thermocline. These structures have traditionally been attributed to secondary Kelvin–Helmholtz (KH) instability (e.g. Woods 1969; Maslowe 1973). Since a bifurcation of this type would induce a cascade of energy to small scales, it has been suggested as an alternative path to turbulence. However, a secondary KH instability need not introduce the three-dimensional motions characteristic of turbulence, so this idea is of questionable validity (Klaassen & Peltier 1985*b*, *c*). We note that Corcos & Sherman (1976) have presented a simple braid model which indicates that secondary KH instability should only occur for Reynolds numbers much larger than those found in Woods' observations.

Early laboratory studies (e.g. Browand 1966; Freymuth 1966; Thorpe 1968) have documented the occurrence of a secondary subharmonic instability that causes neighbouring pairs of vortices to merge. Browand & Winant (1973) furthermore established that the presence of stable stratification can reduce the number of successive occurrences of such pairing, and Winant & Browand (1974) identified the process as a mechanism that greatly accelerates the growth of the shear layer and therefore plays a fundamental role in determining the rate at which momentum is mixed. Koop & Browand (1979) have shown that the average number of pairings expected for a given vortex decreases as the initial stratification is increased. More recent observations by Ho & Huang (1982) and Hernan & Jimenez (1982) demonstrated that, under certain circumstances, more than two vortices may collectively amalgamate in a single interaction.

Von Kármán's pioneering theoretical analysis of the stability of a row of like-signed point vortices (see Lamb 1932) demonstrated that the first subharmonic was the most unstable disturbance in a continuous spectrum. Kelly (1967) considered the stability of a continuous horizontally period vorticity distribution consisting of a parallel flow plus its most unstable eigenfunction as determined by linear theory. Kelly's small-amplitude analysis indicated that pairing might be initiated by a resonance mechanism confined to the neighbourhood of the first subharmonic wavenumber. Subsequent theoretical efforts (e.g. the nonlinear simulations by Patnaik, Sherman & Corcos 1976 and Riley & Metcalf 1980, and the stability analyses of Stuart vortices by Pierrehumbert & Widnall 1982) were therefore directed exclusively toward understanding the behaviour of the first subharmonic.

Our main purpose in the present paper is to provide a detailed analysis of the various transverse secondary instabilities to which two-dimensional finite-amplitude Kelvin–Helmholtz waves are susceptible in one particular region of parameter space. As we shall see, a corresponding analysis of such modes of instability for unstratified

Stuart vortices will provide a good deal of insight into the more complex stratified problem.

2. Finite-amplitude waves in free shear layers

In preparation for analysing their stability, nonlinear two-dimensional Kelvin–Helmholtz wave states were simulated with a numerical finite-difference model based on the anelastic equations of motion for a Newtonian fluid. In this model the thermodynamic variables are calculated as departures from a hydrostatic isentropic background state. In what follows we denote the vertical profile of density associated with this state by $\bar{\rho}(z)$. Since the shear layers considered here are rather shallow compared with the local isentropic scale height, the solutions obtained from the model are very nearly Boussinesq. A detailed description of the numerical model may be found in Peltier *et al.* (1978).

The initial state in general consists of horizontally uniform, stably stratified parallel shear flow plus a linear superposition of its unstable eigenmodes. The horizontally uniform part is of the form

$$u_x = u_0 \tanh\left(\frac{z-\frac{1}{2}H}{h}\right), \tag{2.1}$$

$$u_z = 0, \tag{2.2}$$

$$\theta = \Theta + \theta_0 \tanh\left(\frac{z-\frac{1}{2}H}{h}\right), \tag{2.3}$$

where u_x and u_z denote horizontal and vertical components of the velocity and θ is potential temperature. Θ denotes the potential temperature of the background state, while H represents the vertical extent of the numerical domain. The constants u_0, θ_0 and h appearing in (2.1)–(2.3) correspond to half the velocity difference, half the potential temperature difference, and half the distance across the shear layer respectively. These constants may be combined with the acceleration due to gravity g, the kinematic viscosity ν, and the thermal diffusivity κ, to define the initial Reynolds number $Re = u_0 h/\nu$, the initial bulk Richardson number $Ri = g\theta_0 h/\Theta u_0^2$, and the Prandtl number $Pr = \nu/\kappa$. For the purposes of this paper we shall focus our attention upon a Kelvin–Helmholtz flow with $Re = 300$, $Pr = 1$ and $Ri = 0.07$.

We employ periodic boundary conditions in the streamwise direction for our numerical simulations so that the shear layer evolves in time only. This so-called T-layer problem is, from a numerical standpoint, considerably more tractable than the S-layer problem in which the shear layer originates at a point in space and broadens as the flow evolves downstream. A discussion of the relation between these two problems may be found in the review by Ho & Huerre (1984).

By setting the horizontal domain length of the model (L) equal to the wavelength λ_{KH} of the most unstable Kelvin–Helmholtz mode of the parallel flow according to linear theory ($\alpha_{\mathrm{KH}} = 0.45$, $\lambda_{\mathrm{KH}} = 14$), we obtain wave histories in which the process of vortex amalgamation cannot occur (e.g. see figure 1). This time sequence of KH wave states is then tested for stability with respect to infinitesimal two-dimensional disturbances. The predictions of these analyses are then compared to nonlinear simulations in which the domain length is set equal to $2\lambda_{\mathrm{KH}}$ and $3\lambda_{\mathrm{KH}}$.

Stuart (1967) reported the existence of a family of steady solutions of the two-

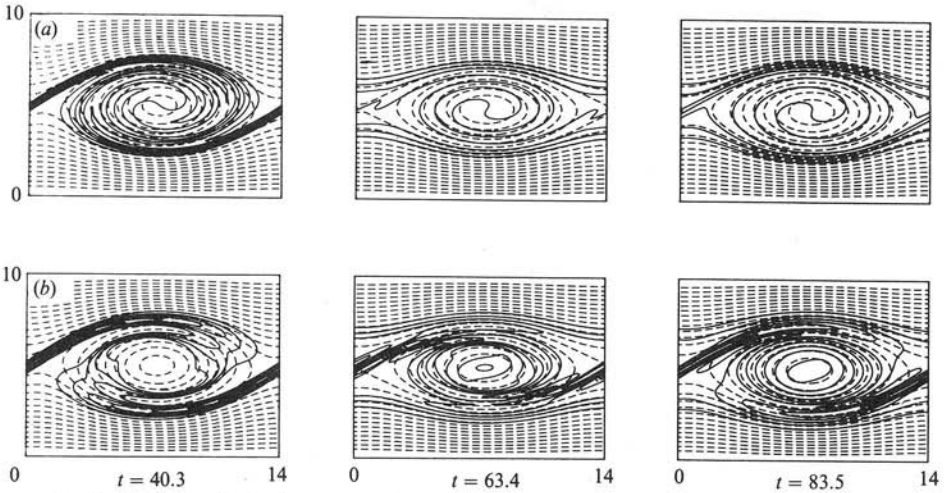

FIGURE 1. Evolution of (*a*) the potential temperature field and (*b*) the vorticity field for a KH simulation in which the initial state is given by (2.1)–(2.3) plus a perturbation of wavelength λ_{KH}. The model domain length $L = \lambda_{KH}$ as well, prohibiting the growth of subharmonics. Fields are shown for key times ($t = 40.3$, 63.4 and 83.5) at which the net wave Reynolds stress vanishes. Dashed contours represent the stream function. $Re = 300$, $Pr = 1$, $Ri = 0.07$.

dimensional Euler equations. In dimensional form, the stream function of these 'Stuart' vortices is given by

$$\psi = u_0 h \ln\left[\cosh\left(\frac{z-\frac{1}{2}H}{h}\right)+A\cos\left(\frac{x}{h}\right)\right], \tag{2.4}$$

while the vorticity has the analytic distribution

$$\zeta = \nabla^2\psi = \frac{u_0}{h}\left[\frac{1-A^2}{\cosh\left(\frac{z-\frac{1}{2}H}{h}\right)+A\cos\left(\frac{x}{h}\right)}\right]. \tag{2.5}$$

The parameter A represents the amplitude of the vortex and may take on values such that $|A| \leqslant 1$. The value $A = 0$ corresponds to the parallel flow $u_x = u_0 \tanh[(z-\frac{1}{2}H)/h]$, while $A = 1$ corresponds to a point vortex. Examples of the vorticity field are shown in figure 2 for various values of A.

The Stuart vortex suffers several limitations as a model of the nonlinear waves that are physically realizable in an unstratified parallel flow. Both experimental (e.g. Winant & Browand 1974) and numerical (e.g. Riley & Metcalfe 1980; Corcos & Sherman 1984) studies of unstratified flow have demonstrated that the shear layer between vortex centres is compressed into thin regions known as the braids, while Stuart vortices show no such structure. The most unstable mode of the hyperbolic tangent shear layer has non-dimensional wavenumber $\alpha = 0.44$, so that the Stuart vortex (wavenumber $\alpha_s = 1$) has about half the wavelength of physically realized disturbances. Since the unstratified parallel flow is stable with respect to infinitesimal disturbances characterized by $\alpha = 1$, there would appear to be no mechanism through which Stuart vortices may develop naturally from small perturbations to parallel flow. Furthermore, unsteady behaviour in the form of vortex nutations (see Klaassen & Peltier 1985*a*) are clearly evident in the unstratified mixing layer observations of Hernan & Jimenez (1982) (especially in their figures 7 and 10). As long as we bear in mind these limitations, however, the Stuart vortex may

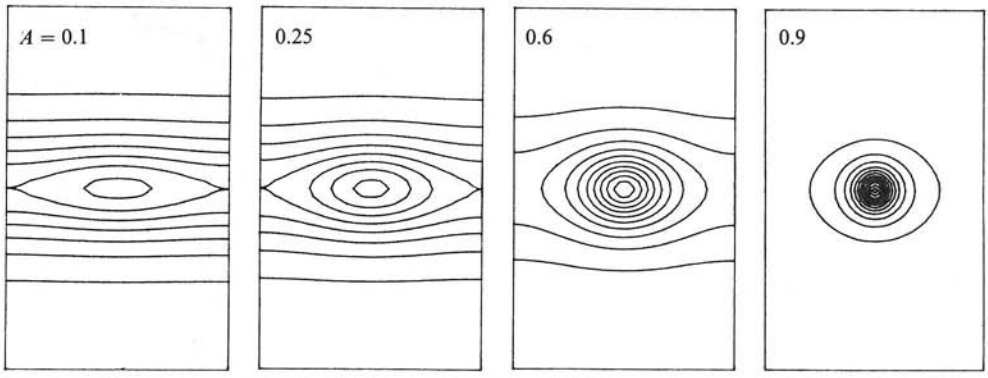

FIGURE 2. The vorticity field for Stuart vortices having various amplitudes A. The vertical domain height is 10 while the horizontal period is 2π. Identical contour levels are employed in each case to illustrate the progression from a weak elliptical vortex to a strongly concentrated, nearly circular vortex as A is increased from 0 to 1. Note the absence of the braids characteristic of the nonlinear disturbances observed in viscous shear layers.

nevertheless provide an instructive and convenient model of the two-dimensional unstratified shear layer.

3. The stability of slowly varying two-dimensional flows

The stability problem for two-dimensional finite-amplitude flow states is formulated by expanding the total dimensional velocity and potential temperature fields as

$$u_i(x,y,z,t) = u_0\,\tilde{u}_i(x,z,t)\,(1-\delta_{i2}) + u_0\,u_i'(x,y,z,t), \tag{3.1}$$

$$\theta(x,y,z,t) = \Theta + \theta_0\,\tilde{\theta}(x,z,t) + \theta_0\,\theta'(x,y,z,t). \tag{3.2}$$

The y-axis ($i = 2$) is oriented in the spanwise direction, normal to the plane of the two-dimensional basic state. Since the two-dimensional finite-amplitude fields denoted by $\tilde{u}_i$ and $\tilde{\theta}$ (which may represent either a nonlinear KH billow or a Stuart vortex) have period $L = 2\pi/\alpha$ in the x-direction, Floquet theory dictates that the perturbations have the form

$$u_i'(x,y,z,t) = \hat{u}_i(x,z,t)\exp[\mathrm{i}(bx+dy)], \tag{3.3}$$

$$\theta'(x,y,z,t) = \hat{\theta}(x,z,t)\exp[\mathrm{i}(bx+dy)], \tag{3.4}$$

where $\hat{u}_i$ and $\hat{\theta}$ also have period L in the x-direction. Note that in this study we shall consider only transverse modes for which $d = 0$, although some comparison with the longitudinal modes discovered in earlier work (Klaassen & Peltier 1985*b*, *c*) will be made.

If the nonlinear states are steady, or vary sufficiently slowly compared to the perturbations, we may write

$$\hat{u}_i(x,z,t) = u_i^{\dagger}(x,z)\,\mathrm{e}^{st}, \tag{3.5}$$

$$\hat{\theta}(x,z,t) = \theta^{\dagger}(x,z)\,\mathrm{e}^{st}, \tag{3.6}$$

where $s = \sigma + \mathrm{i}\omega$, thereby transforming the initial-value problem into an eigenvalue problem. For a steady nonlinear state (such as the Stuart vortex), the exponential temporal dependence is exact, while in the unsteady case (e.g. KH waves), it is an approximation, the validity of which must be subject to *a posteriori* test. We must

discard modes that possess growth rates $\sigma = \mathrm{Re}\{s\}$ that are not large compared with the rate of growth and decay of the nonlinear KH wave σ_{KH}, given by

$$\sigma_{\mathrm{KH}} = \frac{1}{2K}\frac{\mathrm{d}K}{\mathrm{d}t}, \tag{3.7}$$

where

$$K = \frac{1}{2L}\int_0^L \int_0^H \bar{\rho}[(\tilde{u}_x - \bar{u}_x)^2 + \tilde{u}_z^2]\,\mathrm{d}x\,\mathrm{d}z \tag{3.8}$$

is the instantaneous kinetic energy of the nonlinear wave, and

$$\bar{u}_x = \frac{1}{L}\int_0^L \tilde{u}_x\,\mathrm{d}x. \tag{3.9}$$

Substituting perturbation fields of the form (3.3) and (3.4) into the linearized Boussinesq equations yields the following set of stability equations:

$$su_x^\dagger + \tilde{u}_x(\partial_x + \mathrm{i}b)\,u_x^\dagger + \tilde{u}_z\,\partial_z u_x^\dagger + (\partial_x \tilde{u}_x)\,u_x^\dagger + (\partial_z \tilde{u}_x)\,u_z^\dagger = -(\partial_x + \mathrm{i}b)\,p^\dagger + \frac{1}{Re}L_2 u_x^\dagger, \tag{3.10}$$

$$su_y^\dagger + \tilde{u}_x(\partial_x + \mathrm{i}b)\,u_y^\dagger + \tilde{u}_z\,\partial_z u_y^\dagger = -\mathrm{i}dp^\dagger + \frac{1}{Re}L_2 u_y^\dagger, \tag{3.11}$$

$$su_z^\dagger + \tilde{u}_x(\partial_x + \mathrm{i}b)\,u_z^\dagger + \tilde{u}_z\,\partial_z u_z^\dagger + (\partial_x \tilde{u}_z)\,u_x^\dagger + (\partial_z \tilde{u}_z)\,u_z^\dagger = -\partial_z p^\dagger + Ri\,\theta^\dagger + \frac{1}{Re}L_2 u_z^\dagger, \tag{3.12}$$

$$s\theta^\dagger + \tilde{u}_x(\partial_x + \mathrm{i}b)\,\theta^\dagger + \tilde{u}_z\,\partial_z\theta^\dagger + (\partial_x\tilde{\theta})\,u_x^\dagger + (\partial_x\tilde{\theta})\,u_x^\dagger = \frac{1}{Re\,Pr}L_2\theta^\dagger, \tag{3.13}$$

$$(\partial_x + \mathrm{i}b)\,u_x^\dagger + idu_x^\dagger + \partial_z u_z^\dagger = 0, \tag{3.14}$$

$$\mathrm{L}_2 p^\dagger = Ri\,\partial_z\theta^\dagger - 2[(\partial_x\tilde{u}_x)(\partial_x + \mathrm{i}b)\,u_x^\dagger + (\partial_z\tilde{u}_z)\,\partial_z u_x^\dagger + (\partial x\,\tilde{u}_z)\,\partial_z u_x^\dagger + (\partial_z\tilde{u}_z)(\partial_x + \mathrm{i}b)\,u_z^\dagger], \tag{3.15}$$

where the differential operator

$$\mathrm{L}_2 \equiv (\partial_x + \mathrm{i}b)^2 + \partial_z^2 - \mathrm{d}^2. \tag{3.16}$$

The eigensystem (3.10)–(3.15) is solved by expanding $u_x^\dagger$, $u_z^\dagger$, and $\theta^\dagger$ on a Galerkin basis as follows:

$$u_x^\dagger = \sum_{\lambda=-\infty}^{\infty}\sum_{\nu=0}^{\infty} a_{\lambda\nu}\,\mathrm{e}^{\mathrm{i}\lambda\alpha x}\cos\frac{\nu\pi z}{H}, \tag{3.17}$$

$$u_z^\dagger = \sum_{\lambda=-\infty}^{\infty}\sum_{\nu=1}^{\infty} b_{\lambda\nu}\,\mathrm{e}^{\mathrm{i}\lambda\alpha x}\sin\frac{\nu\pi z}{H}, \tag{3.18}$$

$$\theta^\dagger = \sum_{\lambda=-\infty}^{\infty}\sum_{\nu=1}^{\infty} c_{\lambda\nu}\,\mathrm{e}^{\mathrm{i}\lambda\alpha x}\sin\frac{\nu\pi z}{H}. \tag{3.19}$$

(Note that the pressure and spanwise velocity eigenfunctions have been eliminated as discussed in Klaassen & Peltier 1985*b*.) Substituting these Galerkin representations into the stability equations (3.10)–(3.15) and computating the inner

product of each equation with the complex conjugate of the appropriate basis function yields the following closed system of algebraic equations:

$$sa_{\kappa\mu} = \left(I^{(1)}_{\kappa\mu\lambda\nu} - \frac{A_{\lambda\nu}}{Re}\delta_{\kappa\lambda}\delta_{\mu\nu}\right)a_{\lambda\nu} + I^{(2)}_{\kappa\mu\lambda\nu}b_{\lambda\nu} + Ri\left(\frac{iB_\kappa D_\mu}{A_{\kappa\mu}}\right)c_{\kappa\mu}, \tag{3.20}$$

$$sb_{\kappa\mu} = I^{(3)}_{\kappa\mu\lambda\nu}a_{\lambda\nu} + \left(I^{(4)}_{\kappa\mu\lambda\nu} - \frac{A_{\lambda\nu}}{Re}\delta_{\kappa\lambda}\delta_{\mu\nu}\right)b_{\lambda\nu} + Ri\left(\frac{1-D^2_\mu}{A_{\kappa\mu}}\right)c_{\kappa\mu}, \tag{3.21}$$

$$sc_{\kappa\mu} = I^{(5)}_{\kappa\mu\lambda\nu}a_{\lambda\nu} + I^{(6)}_{\kappa\mu\lambda\nu}b_{\lambda\nu} + \left(I^{(7)}_{\kappa\mu\lambda\nu} - \frac{A_{\lambda\nu}}{RePr}\delta_{\kappa\lambda}\delta_{\mu\nu}\right)c_{\lambda\nu}, \tag{3.22}$$

where
$$B_\lambda = \lambda\alpha + b, \quad D_\nu = \frac{\nu\pi}{H}, \quad A_{\lambda\nu} = B^2_\lambda + D^2_\nu + d^2 \tag{3.23}$$

and summation over repeated indices is implied.

The interaction matrices $I^{(n)}_{\kappa\mu\lambda\nu}$ consist of projections of the nonlinear two-dimensional fields onto the Galerkin basis, e.g.

$$I^{(6)}_{\kappa\mu\lambda\nu} = \frac{2}{LH}\int_0^L\int_0^H \exp\left[-i(\kappa-\lambda)\alpha x\right]\sin\left(\frac{\mu\pi z}{H}\right)\sin\left(\frac{\nu\pi z}{H}\right)\partial_z\tilde{\theta}\,dx\,dz. \tag{3.24}$$

Once the expansions (3.17)–(3.19) are truncated at some finite values of the indices, the eigensystem may be solved by standard matrix eigenvalue techniques. By solving (3.20)–(3.22) at various instants in the KH wave history we may identify the time of onset and duration of any secondary instability that the two-dimensional nonlinear wave might support, and obtain another means for assessing the physical importance of a particular mode of instability. Unless the growth rate is sustained for a sufficient length of time, the mode will not reach an amplitude large enough to significantly affect the evolution of the shear layer. Klaassen & Peltier (1985*b*) showed that the expected amplification factor for a particular mode could be satisfactorily estimated by

$$F = \exp\left[\int_0^T \sigma(t)\,dt\right], \tag{3.25}$$

where $[0, T]$ is the interval of non-vanishing σ.

4. Floquet theory and symmetry considerations

The eigensystem defined by (3.10)–(3.15) possesses certain symmetries with respect to the Floquet exponent b. These may be summarized as follows.

I. If s is an eigenvalue at (b, d) with eigenvector $\{u^\dagger_x, u^\dagger_y, u^\dagger_z, \theta^\dagger, p^\dagger\}$ then s^* is also an eigenvalue at $(-b, d)$ with eigenvector $\{u^{\dagger *}_x, -u^{\dagger *}_y, u^{\dagger *}_z, \theta^{\dagger *}, p^{\dagger *}\}$. This may be established by putting $b \to -b$, $u^\dagger_y \to -u^\dagger_y$ and taking the complex conjugate of each of (3.10)–(3.15).

II. The Floquet expansions (3.17)–(3.19), which are of the form

$$f'(x, y, z, t) = \left[\sum_{\lambda=-\infty}^{\infty} f_\lambda(x, z)\,e^{i\lambda\alpha x}\right]e^{i(bx+dy)+st}, \tag{4.1}$$

are invariant under the transformation $b \to b + n\alpha$, where n is an integer. This follows from the periodicity of the Floquet coefficient $f_\lambda(x + 2\pi n/\alpha) = f_\lambda(x, z)$, and the infiniteness of the summation.

III. Properties I and II immediately yield $s(\alpha-b,d)=s^*(b,d)$. These properties permit us to restrict our search of the eigenspace to $0 \leqslant b \leqslant \frac{1}{2}\alpha$.

While the parameter d (which specifies the periodicity of the perturbation in the spanwise direction) may be interpreted as a wavenumber, the same is not true of the parameter b. Each value of b in the continuous range $-\frac{1}{2}\alpha < b \leqslant \frac{1}{2}\alpha$ corresponds to a discrete spectrum of wavevectors, and each component of this spectrum is displaced from a harmonic of the basic state wavenumber by an amount b. Furthermore, we note that the relative amplitudes of the components of this spectrum are determined by the eigensystem, so that the dominant streamwise scale of the perturbation is not necessarily given by $2\pi/b$.

The velocity fields of both Kelvin–Helmholtz waves and Stuart vortices obey the following symmetry:

$$\tilde{u}_x(nL-x,H-z) = -\tilde{u}_x(x,z), \tag{4.2}$$

$$\tilde{u}_z(nL-x,H-z) = -\tilde{u}_z(x,z), \tag{4.3}$$

where L is the period of the nonlinear vortex and n is an integer. The potential temperature field $\tilde{\theta}$ of KH waves obeys

$$\tilde{\theta}(nL-x,H-z) = \tilde{\theta}(x,z). \tag{4.4}$$

As a consequence of these symmetries, the eigenmodes separate (for certain values of b/α) into two distinct groups with even or odd parity under the operator $\mathrm{P}_{xz}^{(n)}$, defined by

$$\mathrm{P}_{xz}^{(n)}\{g(x,z)\} = g(nL-x,H-z). \tag{4.5}$$

It may be shown that these symmetries lead to certain relations between the Galerkin coefficients defined in (3.17)–(3.19). Consider for example the x-velocity perturbation, which may be written in the form

$$u'_x(x,z) = \sum_{\lambda}\sum_{\nu} a_{\lambda\nu}\, \mathrm{e}^{\mathrm{i}(\lambda\alpha+b)x} \cos(\nu\pi z/H) \tag{4.6}$$

with the y- and t-dependence suppressed. Disturbances with horizontal period nL are obtained when the ratio $\beta = b/\alpha = m/n$ is rational (m and n are integers with no common factors). By applying $\mathrm{P}_{xz}^{(n)}\, u'_x = \pm\{u'_x\}$ it may be shown that

$$a_{\lambda\nu} = \pm(-1)^{\nu} a_{-(\lambda+2m/n),\nu} \tag{4.7}$$

The relation (4.7) can be satisfied only when $\lambda+2m/n$ is an integer, i.e. $\beta = 0$ or $\pm\frac{1}{2}$. Thus if $b = 0$ then

$$a_{\lambda\nu} = \pm(-1)^{\nu} a_{-\lambda\nu}, \tag{4.8}$$

while

$$a_{\lambda\nu} = \pm(-1)^{\nu} a_{-\lambda-1,\nu} \tag{4.9}$$

for $b = \frac{1}{2}\alpha$. These relations should be taken into account when formulating the truncation scheme for the expansions (3.17)–(3.19). For the case $b = \frac{1}{2}\alpha$, which is of particular interest in the present paper, any truncation scheme that retains coefficients with $\lambda = \lambda_0$ while discarding those with $\lambda = -\lambda_0 - 1$ violates the symmetry requirements. It will be demonstrated in what follows that such violations can lead, in certain cases, to serious errors in the solution of the eigensystem.

Klaassen & Peltier (1985*b*) employed a modified triangular truncation scheme of the form $2|\lambda|+\nu \leqslant N$ in their investigation of longitudinal modes of instability ($b = 0$). This scheme may be generalized to

$$2|\lambda + b/\alpha| + \nu \leqslant N \tag{4.10}$$

for non-zero b. However, since $|b| \leqslant \frac{1}{2}\alpha$ and ν and N are integers, (4.10) yields only

three different truncation schemes, those corresponding to $\beta = b/\alpha = \frac{1}{2}, 0$, and $-\frac{1}{2}$. For $0 < |b| < \frac{1}{2}\alpha$ neither of the relations (4.8) or (4.9) between the Galerkin coefficients hold and there is no *a priori* rational basis for choosing one scheme over another. The most suitable scheme must be determined empirically by means of convergence tests.

5. Stability of Stuart vortices with respect to transverse disturbances

The problem of the stability of Stuart vortices has been addressed previously by Kelly (1967) for small amplitude and by Pierrehumbert & Widnall (1982) for arbitrary amplitude. The results to be presented in this section augment these earlier analyses. For purposes of comparison, the lengthscale we employ is half that used by Pierrehumbert & Widnall. Consequently a growth rate σ in our units corresponds to a value 2σ in their units, while a Floquet parameter b in our units translates to a value $2b$ in theirs.

Figure 3 illustrates the stability of the Stuart vortex of amplitude $A = 0.1$ with respect to infinitesimal two-dimensional perturbations of arbitrary Floquet parameter. Our analysis reproduces the growth rate of the 'pairing' instability ($b = \frac{1}{2}\alpha_s$) obtained by Pierrehumbert & Widnall (1982). However, figure 3 clearly demonstrates the presence of an additional (more slowly growing) mode not reported by them. The existence of this mode was first recorded in Klaassen & Peltier (1987). The results presented here will elucidate the nature of this instability and permit us to introduce the name 'vortex draining' for the mode. It is also evident in figure 3 that the pairing and draining instabilities each represent the most rapidly amplified components in what are evidently continuous spectra and that the bandwidth of each amalgamation instability is comparable with that of the primary parallel flow instability. (Note that Pierrehumbert & Widnall (1982) did not investigate the stability of transverse perturbations with $b \neq \frac{1}{2}\alpha_s$.)

The rather broad bandwidth of merging instability is of some physical significance. Modes with $|b| < \frac{1}{2}\alpha_s$ in the spectrum contiguous to the pairing instability can lead to the collective amalgamation of more than two vortices. For example, amalgamation modes with $b = \frac{1}{3}\alpha_s$ and $b = -\frac{1}{3}\alpha_s$ (or $b = \frac{2}{3}\alpha_s$ according to III) constitute tripling interactions in which three vortices may combine to form either one or two. (Since $u_y^\dagger = 0$, disturbances having $b < 0$ are identical to their counterparts having Floquet parameter equal to $|b|$.) We may write the Floquet parameter in the form $b = n\alpha_s/m$, where n and m are positive integers possessing no common divisors and $n/m \leqslant \frac{1}{2}$. For the transverse unstable modes of the Stuart vortex shown in figure 3, roughly 98% of the kinetic energy is contained in the components having wavenumbers $k = b = n\alpha_s/m$ and $k = b - \alpha_s = -(m-n)\alpha_s/m$. This characteristic implies that these disturbances will act to reduce the number of vortices in the horizontal distance $2\pi m/\alpha_s$ from either m to n or from m to $m-n$. For the case $m = 2$, the only possible result is $n = m-n = 1$, while for $m = 3$, either one or two vortices may result. The mechanism that determines the outcome for $m > 2$ will be investigated further in §7.

Our analysis indicates that the probability of a particular amalgamation process occurring in an unforced shear layer decreases as the ratio of the minimum number of possible survivors to the number of initial participants decreases. This is consistent with the fact that frequent pairing, and infrequent tripling interactions have been observed in unforced plane mixing layers by Hernan & Jimenez (1982). (Hernan & Jimenez have reported that the number of pairings in their experiments exceeds the

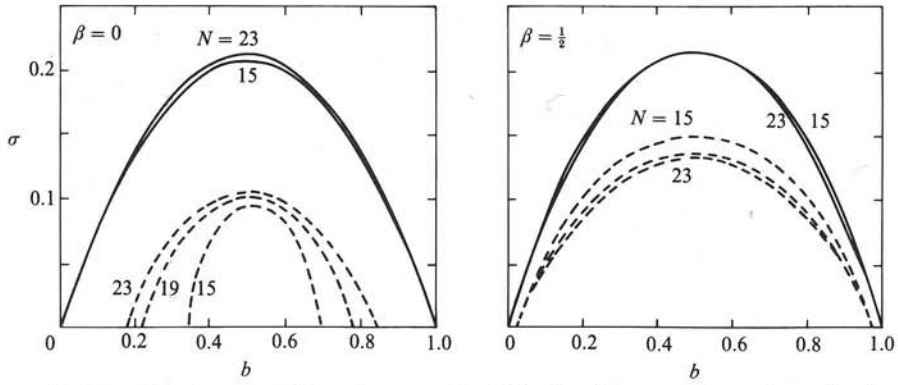

FIGURE 3. Growth rate σ *vs.* Floquet parameter b for the Stuart vortex of amplitude $A = 0.1$. Convergence properties are shown for truncation schemes with $\beta = b/\alpha_s = 0$ and $\frac{1}{2}$; individual curves are labelled with the value of the truncation parameter N. A complete period of b ($0 \leqslant b \leqslant 1$) has been shown to illustrate the lack of symmetry about $b = \frac{1}{2}\alpha_s = \frac{1}{2}$ for the scheme defined by $\beta = 0$. Solid curves represent orbital-merging instability while dashed curves correspond to vortex-draining instability. Both instabilities have non-oscillatory temporal dependence ($\omega = 0$). The most accurate growth rates are for $\beta = \frac{1}{2}$ and $N = 23$.

number of triplings by an order of magnitude.) Our results are also consistent with those of Ho & Huang (1982) who have observed similar processes as well as quadrupling interactions in a forced shear layer. In their experiments the number of vortices participating in the amalgamation process varied with the applied forcing frequency. Forcing at the first subharmonic was found to favour pairing while forcing at the second subharmonic favoured tripling, etc.

The fact that modes close to $b = \frac{1}{2}\alpha_s$ possess nearly the same growth rate as the pairing mode itself means that these modes have a relatively high probability of being realized. Such modes are associated with a lack of sharpness (finite quality factor 'Q') of the vortex merging 'resonance'. For example the mode with $b = \frac{7}{16}\alpha_s$, which has nearly as large a growth rate as the mode with $b = \frac{1}{2}\alpha_s$, would produce a row of vortices having wavelength $\lambda = 2.29\lambda_s$ rather than $\lambda = 2\lambda_s$.

Figure 3 contains growth rate curves obtained using two different truncation schemes, respectively given by

$$2|\lambda| + \nu \leqslant N \quad (\beta = 0) \tag{5.1}$$

and

$$2|\lambda + \tfrac{1}{2}| + \nu \leqslant N \quad (\beta = \tfrac{1}{2}). \tag{5.2}$$

The effectiveness of these two truncation schemes has been tested by examining the convergence characteristics for each as the truncation level N is assigned the values 15, 19 and 23. The growth rates of the amalgamation modes (solid curves) show little variation with truncation level and scheme, indicating that convergence is achieved for this instability. However, the choice of truncation scheme has a significant impact on the growth rates associated with the draining modes (dashed curves). For example, there is some disparity in the instability bandwidth predicted by the two schemes. The scheme $\beta = \frac{1}{2}\alpha_s$ predicts a draining mode bandwidth that is nearly as large as that of the amalgamation instability, and that this bandwidth is essentially independent of truncation level. Conversely the scheme $\beta = 0$ predicts a draining mode bandwidth that is considerably narrower. However, the predicted $\beta = 0$ draining mode bandwidth increases as the truncation level is increased, indicating

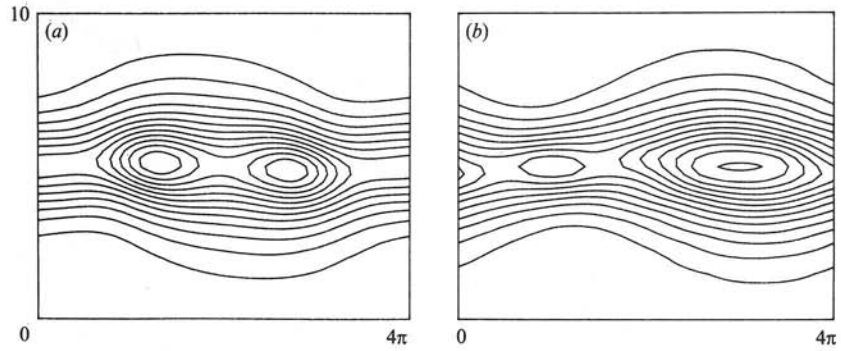

FIGURE 4. A superposition of the (*a*) pairing and (*b*) draining eigenfunctions ($b = \frac{1}{2}$) with the nonlinear vorticity field ($A = 0.10$), shown for two periods of the Stuart vortex. The amplitude of the perturbation vorticity was set to a value 0.25 times the maximum vorticity in the nonlinear field.

that the $\beta = \frac{1}{2}$ scheme with $N = 23$ gives the best estimate of vortex-draining instability growth rates.

The eigenfunctions associated with the two unstable transverse modes of the Stuart vortex for $A = 0.1$ and $b = \frac{1}{2}\alpha_s$ have been superimposed on the nonlinear basic-state vorticity field and displayed in figure 4. The mode in (*a*) moves the left-hand nonlinear vortex up and to the right, while moving the right-hand vortex down and to the left. This motion is consistent with the characteristic orbital motion seen in experiments and simulations of merging vortex pairs, and corresponds to the pairing mode found by Pierrehumbert & Widnall (1982). The additional mode revealed by our analyses lengthens, amplifies and tilts the right vortex, while shortening and depleting (or draining) the left. Hence we have chosen the name draining instability to describe it. The vorticity fields and stream functions associated with the pairing and draining instabilities are shown in figure 5. Evidently the sharp vorticity gradients near $z = \frac{1}{2}H$ and $x = 0, \lambda_s$ are responsible for the slow convergence of the draining mode. The high truncation required to resolve the draining mode could provide an explanation of why Pierrehumbert & Widnall (1982) did not report its occurrence, since they employed a considerably lower maximum truncation level ($N = 8$) than in the present study ($N = 23$).

We note that the overall structure of the two $b = \frac{1}{2}\alpha_s$ modes is essentially similar except for a phase shift by one quarter of the subharmonic wavelength in the horizontal direction, and that each resembles an unstable mode of a parallel flow having a hyperbolic tangent velocity profile. For pairing instability, the long-wave vortex core is centred midway between the short-wave cores, while for draining instability, the centre of the long-wave core is coincident with the centre of the short-wave core that is favoured for growth. It is important to recognize that pairing and draining represent interactions that lead to the merging of vortices through distinctly different routes. In order to distinguish these two different amalgamation processes, we propose that the branch of unstable modes that contains the pairing interaction be referred to as 'orbital merging', while the branch containing the draining interaction be referred to as 'deformational merging'. This nomenclature explicitly recognizes the dominance of vorticity in the former process and the dominance of rate of strain in the latter.

Figure 6 shows the effect of Stuart vortex amplitude on the orbital and

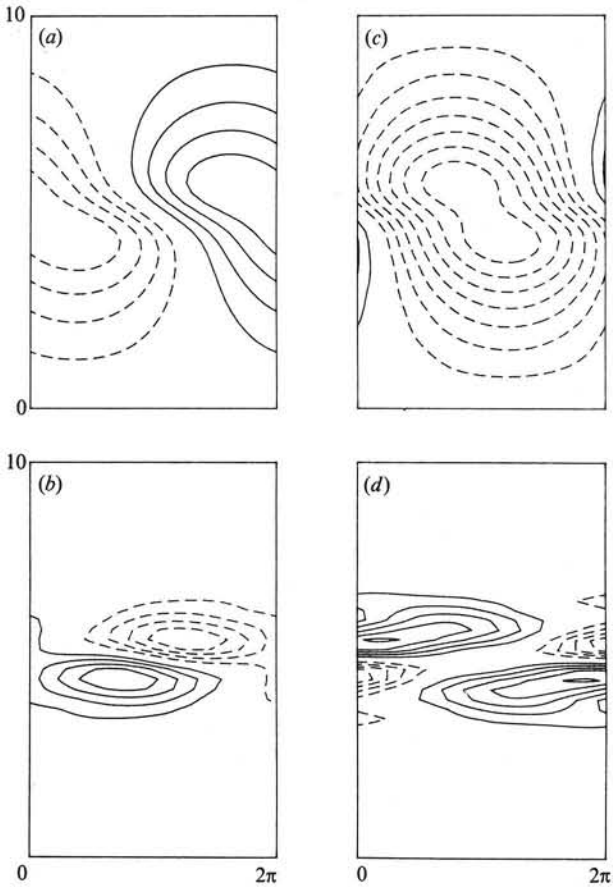

FIGURE 5. Eigenfunctions for the pairing and draining modes ($b = \frac{1}{2}$) of the Stuart vortex with amplitude $A = 0.1$. Pairing (*a*) stream function and (*b*) vorticity field. Draining (*c*) stream function and (*d*) vorticity field. Solid lines represent positive contours, dashed lines represent negative contours. Only the first half-period has been shown in each case.

deformational merging instabilities for Floquet parameters $b = \frac{1}{4}\alpha_s$ and $b = \frac{1}{2}\alpha_s$. Growth rates associated with orbital merging increase slightly as the nonlinear vortex amplitude increases, while those for deformational merging are rapidly diminished by increases in vortex amplitude. It has been argued (Pierrehumbert & Widnall 1982; Corcos & Sherman 1984) that the closest correspondence between the Stuart vortex and the nonlinear disturbances actually observed in free shear layers is obtained for $0.25 \leqslant A \leqslant 0.6$, a range for which orbital-merging growth rates are large and deformational-merging growth rates are small. Thus it is tempting to promote this disparity in growth rates as an explanation of why vortex draining is observed less frequently than orbital pairing. (Hernan & Jimenez 1982 refer to it as a slow 'bleeding' process which constitutes 10% of all merging interactions.) However, one must keep in mind the caveats outlined earlier concerning the substantial structural differences between the Stuart vortex and more realistic nonlinear disturbances. The role played by vortex draining in the evolution of real shear layers will be considered further in what follows.

Figure 6 also provides a comparison of our amalgamation growth rates for the Stuart vortex with two limiting cases that have been examined previously in the

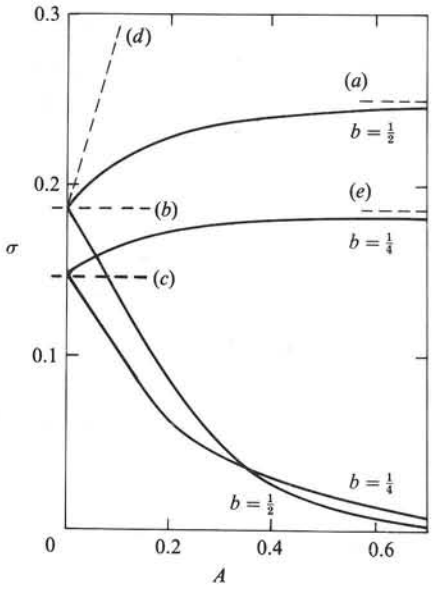

FIGURE 6. Growth rate *vs.* Stuart vortex amplitude for Floquet parameters $b = \frac{1}{4}, \frac{1}{2}$. Pairing growth rates increase slightly as vortex amplitude is increased, while the draining mode is rapidly stabilized by increasing amplitude. The dashed lines marked (*a*) and (*e*) denote the pairing and quadrupling growth rates, respectively, given by Lamb (1932) for a point vortex (the limit $A \to 1$ in the present context). The growth rates associated with instability of hyperbolic tangent parallel flow ($A = 0$) are shown for (*b*) $b = \frac{1}{2}$ and (*c*) $b = \frac{1}{4}$. The line (*d*) denotes the prediction of Kelly (1967) for resonant growth of the first subharmonic of the Stuart vortex.

literature. Our theory in the limit $A \to 1$ provides a rather close correspondence to the growth rates $\sigma = \alpha(1-\alpha)$ predicted by von Kármán's analysis of the stability of a row of like-signed point vortices (Lamb 1932), as illustrated for $\alpha = \frac{1}{2}$ and $\frac{1}{4}$ in figure 6. On the other hand, the small-amplitude resonant interaction theory of Kelly (1967) predicts a value of $\mathrm{d}\sigma/\mathrm{d}A = 0.9648$ for Stuart vortex pairing as $A \to 0$, which is significantly larger than the value 0.50 given by our analysis. Furthermore, Kelly's calculations indicated that orbital merging instability would be confined to a rather narrow band of wavenumbers centred on the subharmonic and having order-A width. This result clearly differs from the order-1 bandwidth given by our calculation (see figure 3). Possible explanations for these differences will be discussed in §8.

6. The stability of Kelvin–Helmholtz billows with respect to transverse disturbances

Klaassen & Peltier (1985*a*) showed that, after reaching maximum amplitude, a KH wave in the absence of subharmonic growth oscillates about a state for which the net Reynolds stress, ξ, given by

$$\xi = \frac{-1}{L} \int_0^H \int_0^L \bar{\rho} \frac{\mathrm{d}\bar{u}_x}{\mathrm{d}z} (\tilde{u}_x - \bar{u}_x)\, \tilde{u}_z \, \mathrm{d}x \, \mathrm{d}z, \tag{6.1}$$

vanishes. The rather small KH wave growth rates (see (3.7)) that obtain during this later period are comparable in magnitude with the frequency with which parcels of fluid orbit the vortex core, and therefore represent a reliable measure of the departure

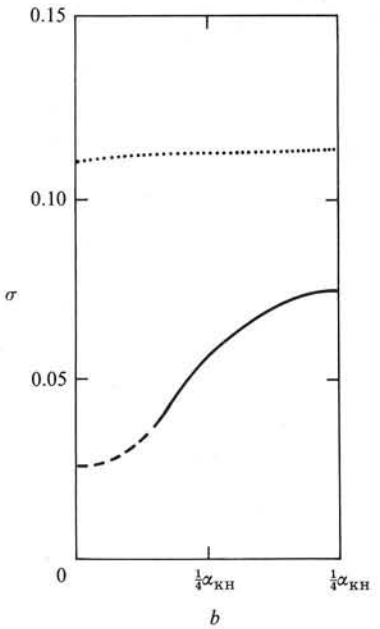

FIGURE 7. Growth rate *vs.* Floquet parameter for transverse unstable modes of the first zero Reynolds stress KH wave state ($t = 40.3$): (····) deformational merging, (——) orbital merging. The instabilities shown are non-oscillatory ($\omega = 0$).

from stationarity. This oscillatory behaviour, which has become known in the literature as vortex nutation, has important implications with respect to the stability analysis. The criterion $\sigma \gg \sigma_{\mathrm{KH}}$ effectively restricts consideration of stability properties to times after (and shortly before) the nonlinear wave attains maximum kinetic energy. The first state for which $\xi = 0$, hereafter referred to as the key time (1), occurs very shortly after maximum KH wave amplitude is attained. The stability characteristics of this state represent a logical point to begin our discussion.

Figure 7 reveals that the KH wave at key time (1) is unstable with respect to two distinct classes of transverse non-oscillatory unstable modes. The growth rate of the fastest growing mode shows little variation with Floquet parameter b, while the growth rate of the other mode exhibits a distinct maximum at the first subharmonic $b = \frac{1}{2}\alpha_{\mathrm{KH}}$. The eigenfunctions corresponding to the more slowly growing of the two modes are illustrated in figure 8 for $b = \frac{1}{2}\alpha_{\mathrm{KH}}$. Comparison with the corresponding unstable modes of the Stuart vortex (see figure 5) indicates that the stream function of this particular instability has the spatial structure and phase required to induce pairing of neighbouring KH vortex centres. Note that the vorticity eigenfunction shows a considerably more intricate spatial structure than the corresponding Stuart vortex eigenfunction (figure 5). That this detailed structure is indeed associated with the KH wave pairing will be demonstrated in §7.

It is worth mentioning that, for the maximum truncation level accessible in the stratified case ($N = 19$), the $\beta = \frac{1}{2}$ truncation scheme (5.2) was needed to provide reasonable convergence of eigenvalues and eigenfunctions. The failure of the $\beta = 0$ scheme (5.1) to produce adequate convergence may be understood as follows. The vorticity field of the pairing eigenfunction consists of alternating thin layers of positive and negative vorticity, a structure represented by Galerkin coefficients $a_{\lambda\nu}$ with small $|\lambda|$ and large ν. The $\beta = 0$ scheme sets $a_{-1,N} = 0$ while retaining $a_{0,N}$ as a

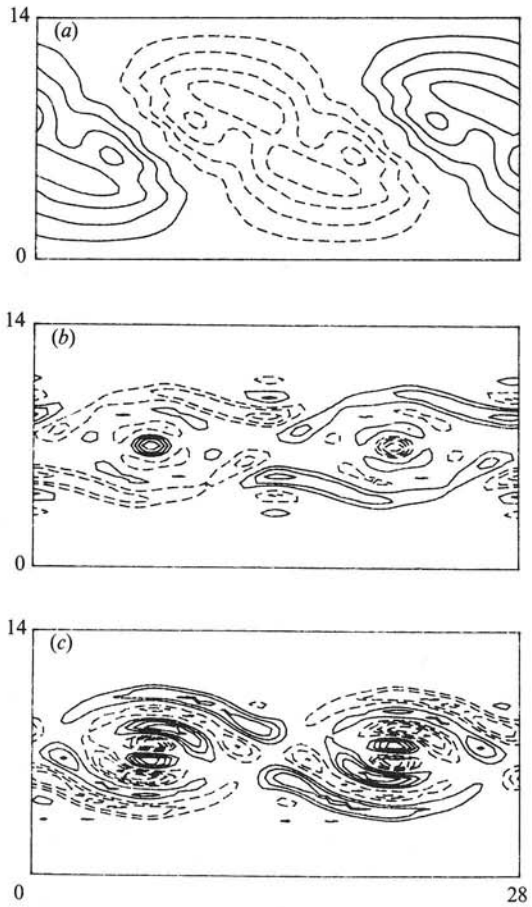

FIGURE 8. (*a*) Stream function, (*b*) potential temperature and (*c*) vorticity eigenfunctions for pairing mode ($b = \frac{1}{2}\alpha_{\mathrm{KH}}$, $d = 0$) at the time the net KH wave Reynolds stress first vanishes ($t = 40.3$). The horizontal domain L corresponds to two KH wavelengths (vortex centres are located at $\frac{1}{4}L$ and $\frac{3}{4}L$).

free parameter, so that the symmetry requirement $a_{-1,N} = \pm(-1)^N a_{0,N}$, (4.9), cannot be satisfied when $a_{0,N}$ still has appreciable magnitude.

The broad bandwidth of the KH orbital merging modes shown in figure 7 demonstrates that tripling, quadrupling, higher-order and intermediate amalgamations are possible in principle (e.g. if the spectrum of background noise is biased in their favour). On intuitive grounds, one would expect no amalgamation in the limit $b \to 0$, as was found in the Stuart vortex case. In the KH case, however, a positive value of σ is found at $b = 0$. This apparently unphysical prediction is explained by the fact that the stability properties of the KH amalgamation mode cannot be reliably determined for $b \leqslant \frac{1}{8}\alpha_{\mathrm{KH}}$ (the dashed portion of the curve in figure 7), simply because the growth rates are not large compared with temporal variations in the KH wave.

Eigenfunctions corresponding to the most unstable transverse mode of the KH wave at key time (1) are shown in figure 9 for the case $b = 0$. This mode is composed of a highly localized counter-rotating vortex doublet (i.e. a dipole distribution) that tends to distort the KH wave braid in the vicinity of the stagnation point. The fact

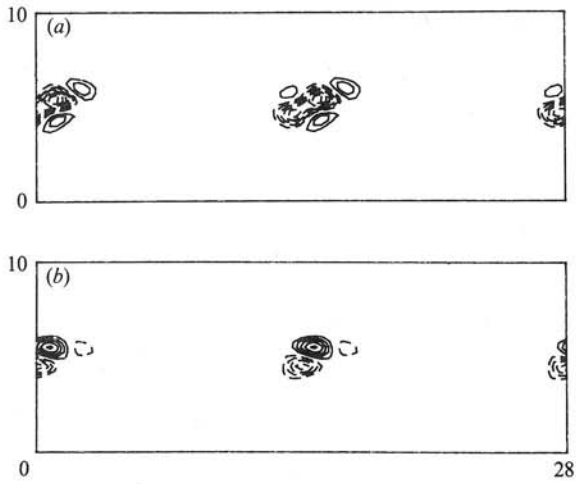

FIGURE 9. (*a*) Potential temperature and (*b*) vorticity eigenfunctions for the braid instability ($b = 0$, $d = 0$) at the first occurrence of zero KH wave Reynolds stress ($t = 40.3$). The horizontal domain length L corresponds to two KH wave periods with vortex centres located at $\frac{1}{4}L$ and $\frac{3}{4}L$.

that the growth rate of this disturbance is nearly independent of the Floquet parameter b simply indicates that variations in structure may occur from one braid to the next in the periodic train of KH billows without significantly affecting the overall growth of the instability. For example, the unstable mode having $b = \frac{1}{2}\alpha_{\mathrm{KH}}$ is very similar in character to the case $b = 0$ shown in figure 9, except that the sign of alternating vortex doublets is reversed. Evidence for the realization of this instability may be seen at $t = 63.4$ in the nonlinear simulation documented in figure 1 (see also figures 7, 8 and 9 of Klaassen & Peltier 1985*c*). It is therefore possible that this mode is responsible for the small-scale wave-like distortions of KH braids observed by Thorpe (1968) in the laboratory and Woods (1969) in the ocean. These observations have traditionally been attributed to a secondary Kelvin–Helmholtz instability originating in the braids.

However, the braid instability that we have discovered here differs from local KH instability in several important respects. For example, only one 'wavelength' is realized, even though the braids appear to possess uniform structure over a distance approximately three times this length. More significantly, the KH eigenfunction consists of a quadrupolar vortex, corresponding to a deformation field that alternately compresses and expands the interface along its length. In contrast, the dipolar vortex structure of the braid instability discovered here initially induces a more or less uniform sinusoidal displacement of the interface. We cannot exclude the possibility that secondary KH instability of the braids may arise for values of the flow parameters that differ significantly from those considered in the present study. However, the braid instability mechanism revealed by our analyses clearly provides a plausible explanation for the observations of Thorpe and Woods, especially since the Reynolds and Richardson numbers characteristic of the flows in their studies are close to the values employed in the present model.

The fact that the instability of figure 9 appears to be associated with the stagnation points located at the midpoints of the braids of the nonlinear wave invites comparison with the stagnation-point instability found by Craik & Criminale (1986). These latter disturbances are Kelvin modes that arise from a constant deformation

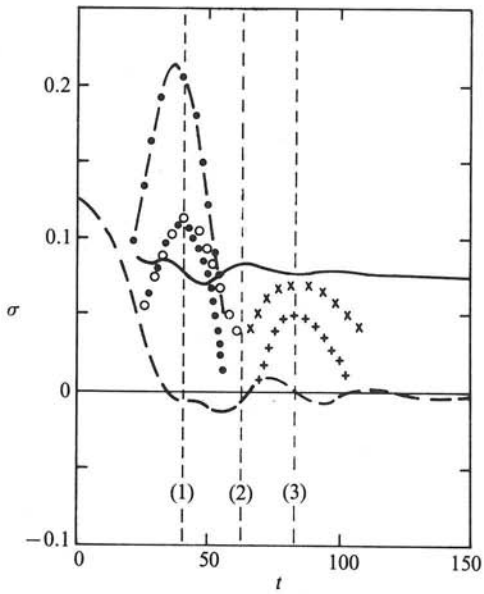

FIGURE 10. The effect of the evolving KH wave on secondary instabilities: – – –, the nonlinear KH wave (σ_{KH}); ——, pairing instability ($b = \frac{1}{2}\alpha_{KH}$, $d = 0$); ○ ○ ○, braid instability ($b = 0$, $d = 0$); ● ● ●, braid instability ($b = \frac{1}{2}\alpha_{KH}$, $d = 0$); – · – · –, longitudinal convective instability ($b = 0$, $d = 3.0$); × × ×, secondary global KH instability ($b = 0$, $d = 3.0$); + + +, vortex-draining instability ($b = \frac{1}{2}\alpha_{KH}$, $d = 0$). Zero net KH wave Reynolds stress occurs at key times (1) $t = 40.3$, (2) 63.4, and (3) 83.5 as marked by the vertical dashed lines.

field and are periodic along the axis of dilatation, whereas the disturbance we have found is an unstable normal mode that arises from a non-uniform deformation field and is localized to the vicinity of the stagnation point.

Figure 10 depicts the variation of the growth rates of several secondary modes of instability as the primary KH flow evolves. The rate of growth σ_{KH} associated with the amplitude of the nonlinear billow has been provided (long dashes) as a reference for judging the applicability of our assumption concerning the existence of a separation between the temporal scales associated with the primary and secondary disturbances. The vertical dashed lines in figure 10 represent the first three successive instants at which the net Reynolds stress $\xi = 0$, and respectively define the first three key times.

The pairing mode ($b = \frac{1}{2}\alpha_{KH}$) shows very little variation with time, indicating that this instability is relatively insensitive to temporal variations in the KH wave. On the other hand, the braid instability (shown for both $b = 0$ and $b = \frac{1}{2}\alpha_{KH}$) is very sensitive to temporal variations in the KH wave, peaking near the key time (1) and decaying before the key time (2). This contrasting behaviour may be understood on the following basis. The pairing mode responds to the large-scale structure of the periodic train of billows, which changes very slowly in these simulations. The imposed domain length $L = \lambda_{KH}$ prevents the occurrence of pairing. However this restriction does not prevent the realization of the braid instability, which achieves a rather small saturation amplitude and then decays. This decay is brought about by nonlinear interactions which destroy those properties of the braid that originally caued the excitation of the secondary instability. Thus the decay of the braid instability's growth rate revealed by our linear theory is simply a measure of this nonlinear modification of the flow in the vicinity of the stagnation point. The

characteristics of the transverse braid instability documented both in our nonlinear simulations and our linear stability analyses indicate that, in the region of parameter space considered here, it is responsible only for a temporary distortion of a highly localized region of the flow.

Figure 10 provides evidence for two further instabilities that occur after the key time (2). The more slowly growing of the two modes (shown here for $b = \frac{1}{2}\alpha_{\mathrm{KH}}$) has the same stream-function structure and phase as the vortex draining instability encountered in our analysis of the stability of Stuart vortices. As in the Stuart vortex case, the fastest growing mode in the continuous spectrum of draining instability occurs at $b = \frac{1}{2}\alpha_{\mathrm{KH}}$ and growth rates vanish in the limit $b \to 0$. The mode with the larger growth rate (shown here for $b = 0$) actually forms a continuous part of the branch associated with pairing instability. We note that the limit $b \to 0$ is singular in the sense that perturbations with $b = 0$ have the same period as the fundamental wave, while perturbations having small $|b|$ possess periods that are many times larger. The mode with $b = 0$ shown in figure 10 has eigenfunctions that closely resemble those of the primary KH instability. Thus it appears that this mode corresponds to a secondary global KH instability. Both the vortex draining and secondary global KH instabilities have a growth rate that is somewhat lower than that associated with pairing and both arise considerably later than the amalgamation instabilities. Thus they are not likely to be of much physical consequence in this particular flow.

Figure 10 also contains the history of the growth rate associated with the most unstable longitudinal mode of the KH wave. This mode, which was described in detail by Klaassen & Peltier (1985*b*), is inherently three-dimensional and corresponds to a Floquet parameter of $b = 0$ and a spanwise wavenumber of $d = 3.0$. It consists of non-oscillatory ($\omega = 0$) convection rolls aligned in the direction of the mean shear and confined to regions of the vortex core in which the initially stable stratification has been overturned. The instability is initiated a short time before the KH wave attains maximum amplitude and decays before the key time (2). We note that for the particular flow parameters considered here the growth rates associated with this instability are nearly twice as great as those found for the pairing or braid instabilities.

The existence of a complex variety of instabilities raises the following question: will any one of these instabilities dominate the subsequent flow evolution, or will each be able to proceed more or less independently? For example, a rapidly growing instability could, through nonlinear processes, modify the KH flow in such a manner as to curtail the realization of instabilities that grow less quickly or are initiated at a later time. For the values of the flow parameters employed in this study it appears that the braid instability will have at most a temporary and somewhat minor impact on the flow in a small region near the stagnation points. On the other hand both the amalgamation and convective instabilities are expected to profoundly affect subsequent flow evolution, the former by increasing the vertical extent of the shear layer, and the latter by leading to the onset of turbulence. The convective instability constitutes a rapid response to a feature of the flow that eventually dissipates (namely the first statically unstable region produced by the overturning billow), while the pairing mode constitutes a somewhat weaker response to a longer-lived feature of the flow (the periodic concentration of vorticity).

7. Two-dimensional nonlinear simulations of vortex amalgamation

In this section we examine the nonlinear evolution of KH waves when the horizontal domain length of the numerical model is set to $L = 2\lambda_{KH}$ and $3\lambda_{KH}$. This permits the growth of subharmonic wave components that are responsible for vortex merging. Such simulations are employed here to verify the results of our linear stability theory, to investigate the sensitivity of the pairing process to initial conditions, to study the flow behaviour after merging is completed, and to simulate tripling interactions.

In order to quantify our results, we find it convenient to partition the kinetic energy of the nonlinear wave into components that may be associated with particular wavenumbers in the Fourier spectrum of the wave. We define these Fourier components according to

$$u(k,z,t) = \frac{1}{L}\int_0^L \tilde{u}_x(x,z,t)\,\mathrm{e}^{-\mathrm{i}kx}\,\mathrm{d}x, \tag{7.1}$$

$$w(k,z,t) = \frac{1}{L}\int_0^L \tilde{u}_z(x,z,t)\,\mathrm{e}^{-\mathrm{i}kx}\,\mathrm{d}x, \tag{7.2}$$

where $k = n\alpha$, $\alpha = 2\pi/L$, $n = 0, 1, 2, \ldots \frac{1}{2}(N-1)$, and N is the number of horizontal grid points employed in the finite-difference model. The kinetic energy of the component with wavenumber k is then defined by

$$E(k) = \frac{1}{1+\delta_{k0}}\int_0^H [u(k,z)\,u^*(k,z) + w(k,z)\,w^*(k,z)]\,\mathrm{d}z, \tag{7.3}$$

and the total kinetic energy is given by

$$E = \frac{1}{L}\int_0^L\int_0^H \left[\frac{\tilde{u}_x^2+\tilde{u}_z^2}{2}\right]\mathrm{d}x\,\mathrm{d}z \approx \sum_{n=0}^{\frac{1}{2}(N-1)} E(n\alpha), \tag{7.4}$$

where the summation has been truncated in accord with the finite resolution of the model. $E(0)$, $E(\frac{1}{2}\alpha_{KH})$, and $E(\alpha_{KH})$ correspond to the energies associated with the mean, subharmonic, and fundamental components of the flow. The amplitude growth rate for the component with wavenumber k is given by

$$\sigma(k) = \frac{1}{2E(k)}\frac{\mathrm{d}E(k)}{\mathrm{d}t}. \tag{7.5}$$

In what follows, we shall see that the time of onset and other characteristics of vortex merging are very sensitive to the flow history that precedes the nonlinear development of the primary wave. In order to quantify these effects, we must establish a criterion for the onset of nonlinear effects, as well as a criterion for distinguishing between forced and unforced shear layers. A linear stability analysis of the initial parallel flow specified by (2.1)–(2.3) dictates that the only unstable modes that can be excited in a system with horizontal period $L = 4\pi/\alpha_{KH} = 2\lambda_{KH}$ are those with wavenumbers $\frac{1}{2}\alpha_{KH}$, α_{KH} and $\frac{3}{2}\alpha_{KH}$. (All other Fourier components of the disturbance lie outside the range of unstable modes $0 < \alpha \lesssim 2\alpha_{KH}$.) Figure 11 illustrates the evolution of $E(k)$ and $\sigma(k)$ for each of these three components in a $2\lambda_{KH}$ domain length simulation initiated with a white-noise field superimposed on the parallel flow such that $E(k \neq 0) \sim 10^{-5}$ at $t = 0$. At first all components decay. However growth rates for $k = \frac{1}{2}\alpha_{KH}$, α_{KH}, and $\frac{3}{2}\alpha_{KH}$ increase rapidly until the

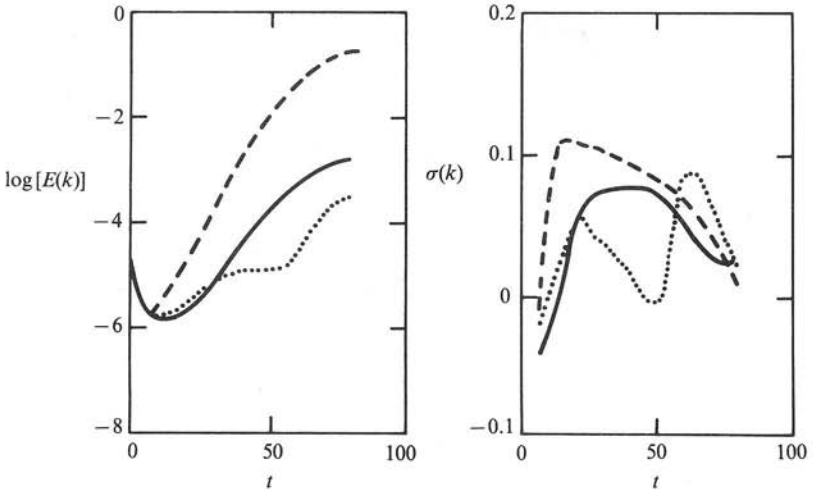

FIGURE 11. Evolution of (*a*) the kinetic energy and (*b*) the growth rate associated with the Fourier components $k = \frac{1}{2}\alpha_{\mathrm{KH}}$ (——), α_{KH} (– – –), and $\frac{3}{2}\alpha_{\mathrm{KH}}$ (· · · · ·), for a nonlinear simulation in which white noise having spectral kinetic energy density $E(k) \approx 10^{-5}$ is superimposed on the initial parallel flow. (The model domain length is equal to $2\lambda_{\mathrm{KH}}$.)

values dictated by linear stability theory are respectively attained. At these individual times the components have 'locked on' to the appropriate eigenfunctions. Thereafter, the $\sigma(k)$ decrease at rates that are dictated by viscous diffusion of the mean flow.

Mean flow diffusion acts to increase the depth of the shear layer, and effectively shifts the entire unstable spectrum (including the fastest growing mode) to longer wavelengths. Thus, if the 'initial' disturbance is sufficiently small and the viscosity is sufficiently large, mean flow diffusion can shift the dominant wavelength of the growing disturbance to substantially larger values before nonlinear effects become important. In the absence of evidence to the contrary it is reasonable to expect that the disturbance with largest amplitude at the time nonlinear effects become important will be the one to impose its wavelength on the shear layer. This hypothesis is given some credence by the fact that mean flow diffusion is substantially reduced by the emergence of a strongly nonlinear wave (see figure 1 of Klaassen & Peltier 1985*a*).

In order to achieve the closest possible correspondence with the physical processes occurring in unforced natural flows, it is therefore necessary to initialize a numerical simulation with the amplitude of the fastest-growing mode of the parallel flow set to a value slightly smaller than that required to induce nonlinear effects. The amplitude corresponding to this nonlinear threshold may be determined from figure 11. At time $t = 50$ the growth rates for the subharmonic and fundamental decrease rather sharply, and $\sigma(\frac{3}{2}\alpha_{\mathrm{KH}})$ abruptly increases. This behaviour indicates that the amplitude of the fundamental is large enough to introduce significant nonlinearity into the layer. We have been able to identify $E(\alpha_{\mathrm{KH}}) \approx 10^{-2}$ as the critical threshold for the onset of nonlinear effects over a fairly broad range of Reynolds number ($10^2 < Re < 10^3$). Consequently, an initial value of $E(\alpha_{\mathrm{KH}}) \approx 2 \times 10^{-3}$ was chosen for the remainder of our simulations. The corresponding initial values for $E(\frac{1}{2}\alpha_{\mathrm{KH}})$ and $E(\frac{3}{2}\alpha_{\mathrm{KH}})$ may vary considerably, depending on the shape of the particular spectrum of noise responsible for exciting the instability. As a specific example of the values

to be expected, the simulation shown in figure 11 gives $E(\frac{1}{2}\alpha_{\mathrm{KH}}) = \frac{1}{50}E(\alpha_{\mathrm{KH}})$ (an amplitude ratio of 1:7) and $E(\frac{3}{2}\alpha_{\mathrm{KH}}) = \frac{1}{200}E(\alpha_{\mathrm{KH}})$ (an amplitude ratio of 1:14) at the time when $E(\alpha_{\mathrm{KH}}) = 2\times10^{-3}$.

It is important, however, to recognize that there is an upper limit to the ratio $E(\frac{1}{2}\alpha_{\mathrm{KH}})/E(\alpha_{\mathrm{KH}})$ that may be expected to occur in an unforced shear layer. Clearly, the time required for an individual Fourier component to lock on to the corresponding growing eigenfunction must be inversely proportional to the growth rate. Figure 11 illustrates this concept quite nicely: the fastest-growing mode $k = \alpha_{\mathrm{KH}}$ is the first to lock on, while the components $k = \frac{1}{2}\alpha_{\mathrm{KH}}$ and $k = \frac{3}{2}\alpha_{\mathrm{KH}}$ (which have nearly equal growth rates) simultaneously lock on at a somewhat later time. The data in figure 11 indicate that, owing to the difference in lock-on times, $E(\alpha_{\mathrm{KH}})$ amplifies by a factor of about 10 before the subharmonic even begins to grow. We have verified that this threefold gain in the amplitude of the fundamental relative to the subharmonic is insensitive to the amplitude of the initial noise field in the linear regime, and thus constitutes a lower bound for the value of $[E(\alpha_{\mathrm{KH}})/E(\frac{1}{2}\alpha_{\mathrm{KH}})]^{\frac{1}{2}}$ that can be expected at the nonlinear threshold in an unforced layer. (Observational evidence (e.g. Ho & Huang 1982; Miksad 1972) indicates that this amplitude ratio is often as high as 30 in unforced free shear layers.) In recent numerical simulations of the pairing process in unstratified free shear layers, Corcos & Sherman (1984) have employed an initial amplitude ratio of 1:2 between the subharmonic and the fundamental. According to our criterion, these latter simulations correspond to a forced shear layer and therefore favour the early onset of pairing.

Figure 12 demonstrates the effect that 'forced' and 'unforced' initial conditions have on the timing of the pairing process. Both simulations have the initial kinetic energy of the fundamental $E_0(\alpha_{\mathrm{KH}}) = 2\times10^{-3}$, a value slightly smaller than that required to induce significant nonlinear effects. For the forced simulation shown in figure 12(*a*), we employed the initial values

$$E_0(\tfrac{1}{2}\alpha_{\mathrm{KH}}) = E_0(\tfrac{3}{2}\alpha_{\mathrm{KH}}) = \tfrac{1}{4}E_0(\alpha_{\mathrm{KH}}) \tag{7.6}$$

(similar to the values employed by Corcos & Sherman 1984), while for the unforced simulation of figure 12(*b*) we imposed the initial values

$$E_0(\tfrac{1}{2}\alpha_{\mathrm{KH}}) = E_0(\tfrac{3}{2}\alpha_{\mathrm{KH}}) = \tfrac{1}{100}E_0(\alpha_{\mathrm{KH}}). \tag{7.7}$$

For the forced initialization (7.6), the fundamental KH disturbance is barely able to impose its own identity on the flow before it is overwhelmed by subharmonic growth. In contrast, the fundamental mode in the unforced simulation dominates the flow for a considerable length of time before the nonlinear effects of pairing become evident.

Both simulations shown in figure 12 were initialized with $k = \frac{1}{2}\alpha_{\mathrm{KH}}$ and $\frac{3}{2}\alpha_{\mathrm{KH}}$ eigenfunctions of the parallel flow adjusted so that their phases matched those of the respective components of the pairing eigenfunction shown in figure 8. In an unforced shear layer these waves arise out of random noise so that their relative phases are arbitrary, at least in the small-amplitude regime. Thus the particular phases chosen for the simulations shown in figure 12 both favour the early onset of the pairing process. To test the sensitivity of the onset of pairing to the initial phase of the waves with $k = \frac{1}{2}\alpha_{\mathrm{KH}}$ and $k = \frac{3}{2}\alpha_{\mathrm{KH}}$ we have performed several additional simulations.

In figure 13 we display the evolution of $E(k)$ for an 'antipairing' initialization in which both the $k = \frac{1}{2}\alpha_{\mathrm{KH}}$ and the $k = \frac{3}{2}\alpha_{\mathrm{KH}}$ waves are directly out of phase with the respective components of the pairing eigenfunction, a $\frac{1}{2}\pi$ phase shift in each case. For this simulation, the initial amplitudes were set according to the unforced values (7.7).

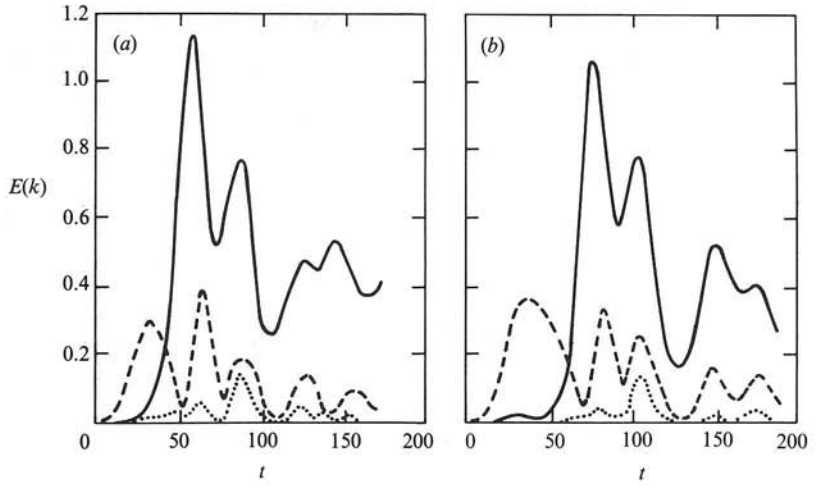

FIGURE 12. Evolution of the kinetic energy $E(k)$ for nonlinear simulations having $L = 2\lambda_{KH}$. Growing eigenfunctions with relative kinetic energies given by $E(\frac{1}{2}\alpha_{KH}):E(\alpha_{KH}):E(\frac{3}{2}\alpha_{KH}) = (a)\ \frac{1}{4}:1:\frac{1}{4}$ (see (7.6)) and $(b)\ \frac{1}{100}:1:\frac{1}{100}$ (see (7.7)) are superimposed on the initial parallel flow. $k = \frac{1}{2}\alpha_{KH}$ (——), α_{KH} (– – –), $\frac{3}{2}\alpha_{KH}$ (· · ·). Initial relative phases are adjusted to match those associated with the pairing instability.

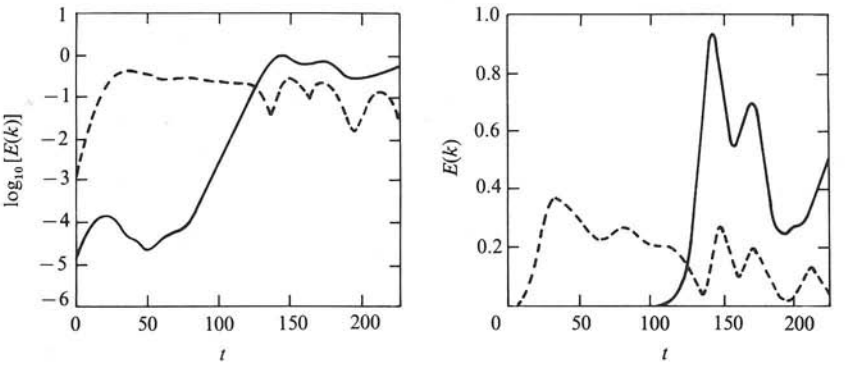

FIGURE 13. Evolution of the kinetic energy $E(k)$ for a simulation in which the initial phases of the $k = \frac{1}{2}\alpha_{KH}$ and $k = \frac{3}{2}\alpha_{KH}$ waves are shifted by $\frac{1}{2}\pi$ radians relative to the values required for pairing instability. $E(\frac{1}{2}\alpha_{KH})$ (——), and $E(\alpha_{KH})$ (– – –). Initial disturbance amplitudes as for the simulation in figure 12(*b*) (see (7.7)).

In the unstratified steady Stuart vortex case such a linear disturbance would tend to induce vortex-draining instability. However, for a KH wave with initial stratification given by $Ri = 0.07$, draining instability onsets very late in the wave history (after the key time (2) in figure 10). Thus, directly after the fundamental mode crosses the nonlinear threshold, the imposed initial subharmonic does not project onto any unstable mode of the nonlinear primary wave, and the subharmonic kinetic energy $E(\frac{1}{2}\alpha_{KH})$ begins to decay. After a considerable lapse of time, however, the subharmonic does eventually begin to grow. An examination of the vorticity and potential temperature fields shows that this late subharmonic growth is associated with pairing instability rather than vortex draining.

This result can be better understood by examining the evolution of the horizontal

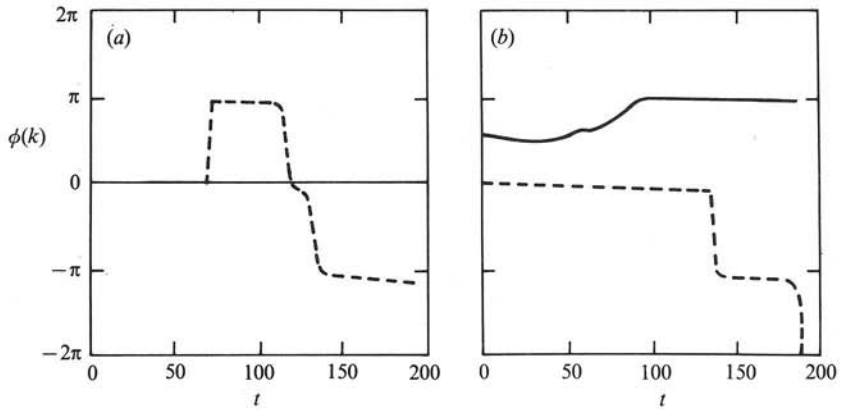

FIGURE 14. Evolution of the central phase (k) of the stream function for the simulations shown in (a) figure 12(b), and (b) figure 13. $k = \frac{1}{2}\alpha_{\mathrm{KH}}$ (——) and $k = \alpha_{\mathrm{KH}}$ (– – –).

phase $\phi_k(z,t)$ of each Fourier component of the stream function ψ. We define this phase according to

$$\psi(x,z,t) = \sum_k \psi_k(z,t)\,\mathrm{e}^{\mathrm{i}[kx+\phi_k(z,t)]}. \tag{7.8}$$

Of particular interest is the phase at the centre of the shear layer, namely,

$$\phi(k) \equiv \phi_k(z = \tfrac{1}{2}H, t). \tag{7.10}$$

The evolution of this central phase for simulations initialized with both pairing and antipairing phases is shown in figure 14. For the pairing-phase initialization (figure 14a), the phase of the subharmonic remains constant for all time. (It is worth mentioning that the rapid reversal in the phase of the fundamental that occurs at $t = 65$ exactly coincides with the onset of nonlinear effects in the pairing process.) For the antipairing initialization (shown in figure 14b) the phase of the subharmonic remains near the value $\frac{1}{2}\pi$ until $t = 50$ and then begins a steady migration toward the value required for pairing. (Note that either $\phi(\frac{1}{2}\alpha_{\mathrm{KH}}) = 0$ or π can lead to pairing. A phase shift of π radians only selects the right- or left-hand neighbour of a particular vortex to engage in the merging process.) By $t = 70$, the subharmonic phase has migrated far enough for pairing instability to take over. According to figure 10, this process is completed well before the onset of vortex-draining instability, so that the outcome is orbital rather than deformational merging.

The outcome of our antipairing simulation (figure 13) differs from the corresponding simulation performed by Patnaik *et al.* (1976) for the same value of the stratification ($Ri = 0.07$). In their simulation, setting the initial subharmonic component directly out of phase with respect to the pairing eigenfunction led to a 'shredding interaction' in which *both* the fundamental and the subharmonic decayed. From their figure 16, the subharmonic amplitude apparently never exceeds that of the fundamental during this process. This rather different outcome is evidently due to the lower Reynolds number ($Re = 50$) employed.

An antipairing simulation has been performed by Riley & Metcalfe (1980) for the case of an unstratified shear layer (see also the review by Ho & Huerre 1984). This simulation produced an interaction in which the vorticity of one of the fundamental-mode cores was gradually transferred along the developing large-scale braid to its

nearest neighbours. Recall that the vortex-draining instability revealed by our linear stability analyses of Stuart vortices was found to produce a similar interaction (see figures 3 and 4 and the relevant discussion in §5). Thus Riley & Metcalfe's nonlinear simulation provides direct evidence that vortex-draining instability may be excited in unstratified shear layers, although we note that the initial relative amplitude of the subharmonic and fundamental they employed was characteristic of a forced layer (see their figure 15). Our stability analyses have shown that deformational merging interaction is due to a supercritical Hopf bifurcation that is closely related to orbital vortex merging, and our nonlinear simulations have shown that it is not likely to play a significant role in the evolution of moderately stratified free shear layers.

If the initial subharmonic phase is set to a value intermediate between the pairing and antipairing values, vortex merging begins at some time later than in the simulation shown in figure 12(*b*) and at some time earlier than in the simulation shown in figure 13. Further simulations (not shown here) have demonstrated that the relative phase of the component $k = \frac{3}{2}\alpha_{\mathrm{KH}}$ can also play a role in determining the time at which pairing onsets. If one matches the initial $\phi(\frac{3}{2}\alpha_{\mathrm{KH}})$ to the pairing value and shifts the initial $\phi(\frac{1}{2}\alpha_{\mathrm{KH}})$ to the antipairing value, the interaction between the components $k = \alpha_{\mathrm{KH}}$ and $k = \frac{3}{2}\alpha_{\mathrm{KH}}$ generates a subharmonic component with the phase required to excite pairing instability. In this case the onset of pairing significantly precedes that observed in figure 13. The evidence we have accumulated is consistent with the concept that it is the projection of the disturbance field on the pairing eigenfunction at the time nonlinear effects first become important in the layer that ultimately determines the time at which the subharmonic amplitude surpasses that of the fundamental. The simulations shown in figures 12(*b*) and 13 give rough indications of the lower and upper temporal limits for the onset of pairing in an unforced shear layer. The rather large variability in the onset of vortex pairing has important implications with respect to the competition between pairing and the longitudinal convective instability. From figure 10, it is clear that pairing can be excited at roughly the same time as the latter instability, although pairing is rather unlikely to precede it. If initial conditions are unfavourable for pairing, longitudinal convective instability may achieve finite amplitude first. If it then modifies the flow in such a way as to inhibit vortex merging, pairing could be prevented altogether.

The growth rates $\sigma(k)$ calculated from our nonlinear simulations according to (7.5) can be used to verify the results of our linear stability analyses (§6). This comparison tests the validity of our assumption concerning the separation between the timescales of the primary and secondary disturbances. Figure 15 illustrates such a comparison for the three simulations shown previously in figures 12(*a*, *b*) and 13. In each case there exists a period of time for which the growth rate of the subharmonic $\sigma(\frac{1}{2}\alpha_{\mathrm{KH}})$ calculated from the nonlinear simulations is nearly constant and very close to the pairing instability values predicted by our linear theory. We note that the calculation of $\sigma(\frac{1}{2}\alpha_{\mathrm{KH}})$ is not able to distinguish between the excitation of the braid and pairing instabilities in the nonlinear simulations. However the highly localized character of the braid instability would tend to limit its ability to extract energy from the KH wave so that $\sigma(\frac{1}{2}\alpha_{\mathrm{KH}})$ is expected to be a fairly accurate measure of the pairing growth rate.

A much more stringent test of our linear stability analysis is provided by a comparison of the predicted pairing instability eigenfunctions (figure 8) with the actual spatial structure of the pairing component in a nonlinear KH wave simulation. This pairing component may be defined as the difference between the

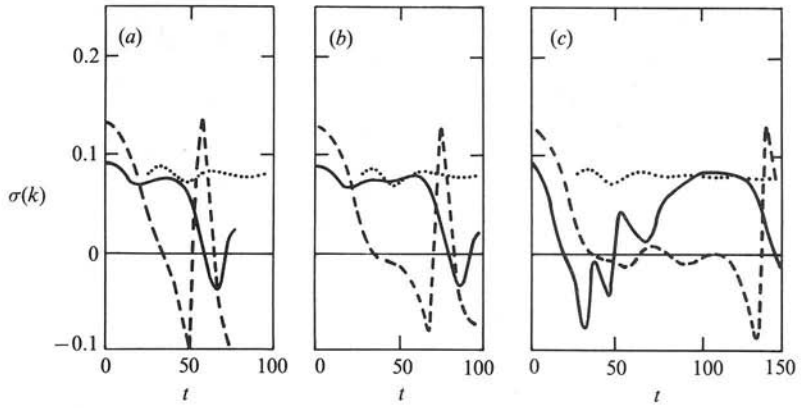

FIGURE 15. Comparison between the pairing-instability growth rates (· · · · ·) predicted by our linear theory and the growth rate $\sigma(\frac{1}{2}\alpha_{\mathrm{KH}})$ (——) of the subharmonic component in a nonlinear simulation of pairing KH waves. The former results were obtained by analysing the stability of the simulation illustrated in figure 1 with respect to infinitesimal perturbations, while the latter were calculated from the nonlinear simulations corresponding to figures (*a*) 12(*a*), (*b*) 12(*b*), and (*c*) 13. In each case the growth rate of the fundamental mode $\sigma(\alpha_{\mathrm{KH}})$ is shown as a point of reference (– – –).

flow fields calculated in a KH wave simulation with period $L = 2\lambda_{\mathrm{KH}}$ and those constructed from two periods of a simulation with $L = \lambda_{\mathrm{KH}}$. (Pairing instability cannot occur in the latter model configuration.) The difference fields corresponding to the eigenfunctions of figure 8 are displayed in figure 16. The agreement between the two stream functions is rather impressive, particularly if one considers the close correspondence between the small-scale details of the fields. Although the agreement is not quite as close for the potential temperature and vorticity fields, the dominant features, such as the alternating layers of positive and negative perturbations, compare well.

The fact, dictated by Floquet theory, that pairing instability involves the excitation of a *spectrum* of horizontal components that grow in unison rather than the amplification of only the first subharmonic component is illustrated in figure 17. At the time that the fundamental component achieves its maximum kinetic energy (figure 17*a*), the spectral amplitudes are clearly separated into two distinct parts, the first comprising the fundamental and its higher harmonics, and the second comprising the subharmonic and its odd harmonics. As pairing proceeds, these two separate spectra blend together, forming a single monotonic spectrum at the time the subharmonic achieves its maximum kinetic energy (figure 17*c*).

Figure 18 shows the evolution of the potential temperature field and the stream function during the course of a pairing event with the initialization (7.7). Figure 18(*a*) confirms the pre-eminence of the fundamental component of the KH wave at the time it achieves maximum amplitude. By the time $E(\frac{1}{2}\alpha_{\mathrm{KH}}) = E(\alpha_{\mathrm{KH}})$, (figure 18*b*), the two vortices have moved closer together and have begun to execute the relative orbital motion characteristic of pairing. At the time of maximum subharmonic amplitude (figure 18*c*), remnants of the parent vortices can still be discerned. In figure 18(*d*), these remnants have disappeared, and the wave height is nearly 2.5 times the original depth of the shear layer. The overturning fluid extrudes so far into the high-speed streams on either side of the shear layer that it is drawn out into thin, nearly horizontal layers (frames *d*–*f*), indicating that a substantial transfer of energy back to the mean flow has occurred (see also figure 19). This

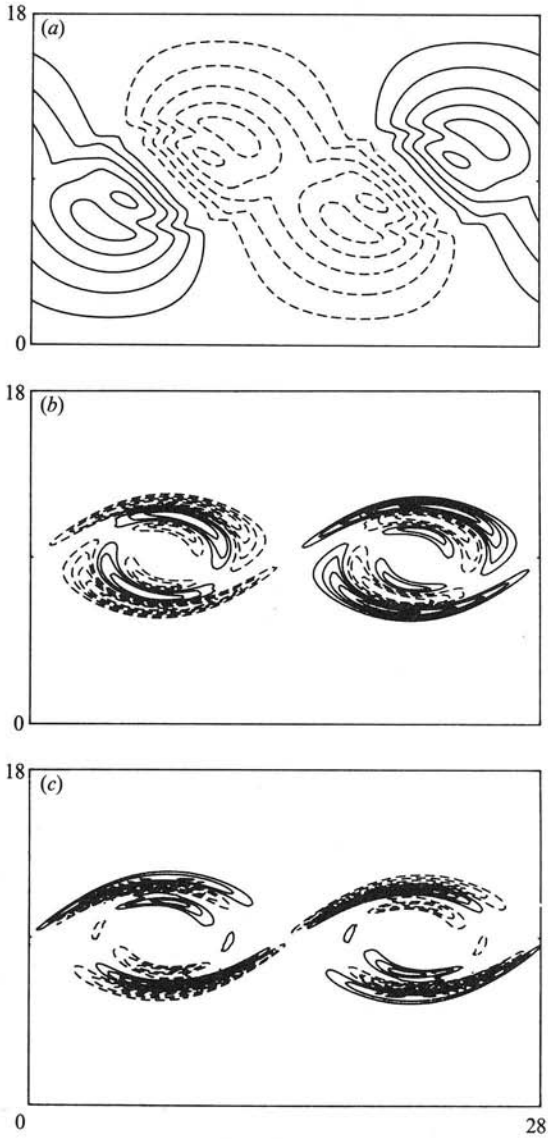

FIGURE 16. By subtracting the flow fields corresponding to a KH wave simulation with domain length $L = 2\lambda_{KH}$ (in which pairing occurs) from those corresponding to two periods of a simulation with domain length $L = \lambda_{KH}$ (in which amalgamation cannot occur), we isolate that part of the flow associated with the pairing process. The results presented here for (*a*) stream function, (*b*) potential temperature, and (*c*) vorticity correspond to $t = 40.3$ and should be compared with the eigenfunctions shown in figure 8. Solid lines correspond to positive values, while dashed lines correspond to negative values.

reinforcement of the mean shear results in the excitation of secondary KH instability in the lower-left and upper-right regions of the paired wave (figure 18*f*).

It has been shown by Klaassen & Peltier (1985*a*) that for the case in which subharmonic growth is prevented, an oscillatory exchange of energy occurs between the wave and the mean shear flow. The effect that vortex pairing has on this energy cycle is illustrated in figure 19, which shows the evolution of the mean, subharmonic,

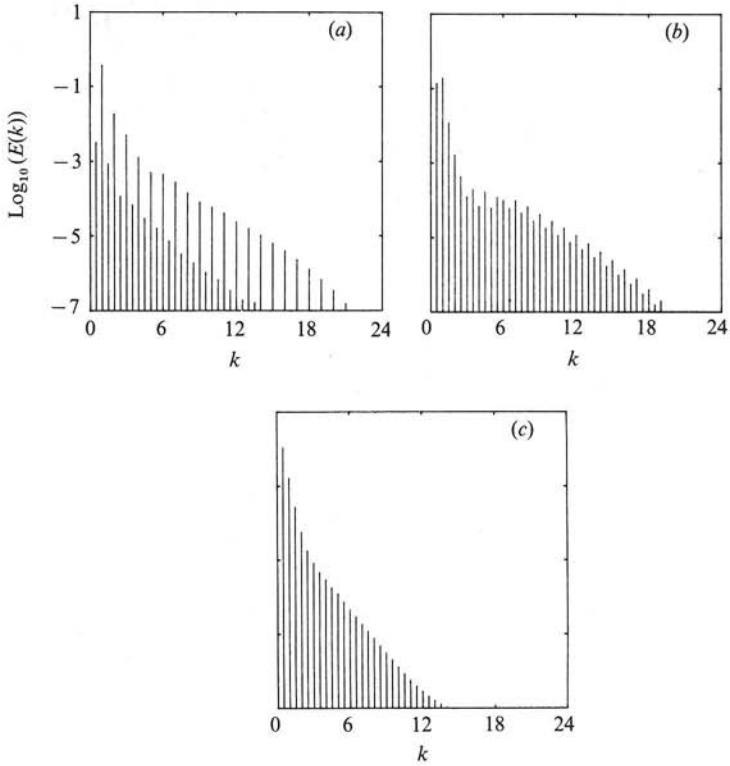

FIGURE 17. Kinetic energy spectra $E(k)$ for a pairing KH wave, shown for the following times: (*a*) maximum $E(\alpha_{\mathrm{KH}})$, $t = 34.6$; (*b*) $E(\alpha_{\mathrm{KH}}) = E(\frac{1}{2}\alpha_{\mathrm{KH}})$, $t = 58.8$; (*c*) maximum $E(\frac{1}{2}\alpha_{\mathrm{KH}})$, $t = 76.1$. The data correspond to the simulation shown in figure 18. The wavenumber axis is labelled in units of $\frac{1}{2}\alpha_{\mathrm{KH}}$.

and fundamental components of the wave kinetic energy (defined by (7.3)), as well as the potential energy defined by

$$\bar{P} = -\frac{1}{L}\int_0^L \int_0^H z\left(\frac{\theta - \Theta}{\theta_0}\right) \mathrm{d}x\,\mathrm{d}z. \tag{7.10}$$

It is evident that energy oscillations continue throughout the pairing process, and represent an even more pronounced feature of the flow after pairing has been completed.

A time series analysis of the total wave kinetic energy reveals the presence of an oscillation with a non-dimensional period $\tau \approx 56$ in the simulations with $L = \lambda_{\mathrm{KH}}$ (no pairing). The same analysis of the simulation shown in figures 12(*b*) and 19 ($L = 2\lambda_{\mathrm{KH}}$) shows the presence of an additional period $\tau \approx 24$. These periods can also clearly be seen in the temporal traces of $E(\frac{1}{2}\alpha_{\mathrm{KH}})$ and $E(\alpha_{\mathrm{KH}})$ shown in figure 19. Thus at the same time as pairing introduces a longer spatial period (the first subharmonic of the primary wave) into the layer, it also excites a shorter temporal period (which is very nearly equal to the first harmonic of the energy cycle). Subharmonic growth involves a substantial increase in wave height which permits the entrainment of fluid from the high-speed streams that lie above and below the original shear zone. The mixing of this high-momentum fluid into the billow is responsible for the introduc-

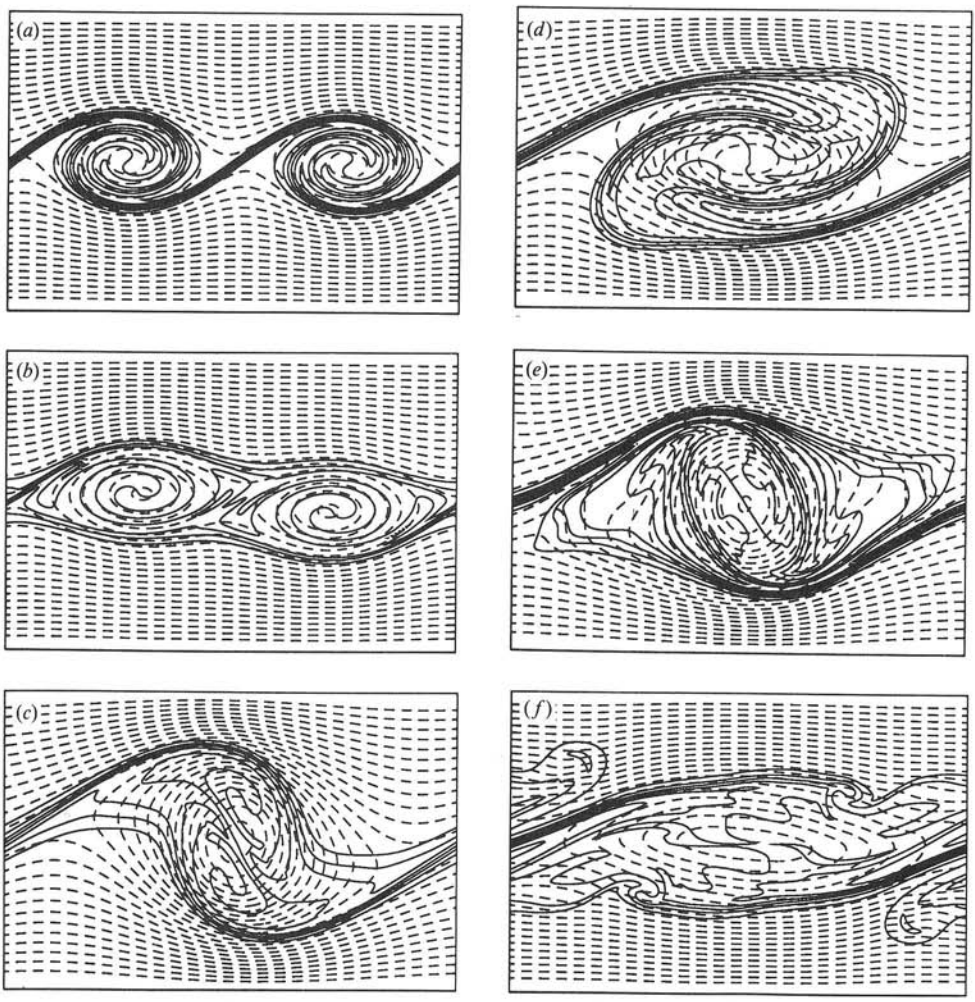

FIGURE 18. Contours of the potential temperature field (solid) overlayed on the stream function (dashed) for a pairing KH wave, shown for (*a*) maximum $E(\alpha_{\mathrm{KH}})$, $t = 34.6$; (*b*) $E(\frac{1}{2}\alpha_{\mathrm{KH}}) = E(\alpha_{\mathrm{KH}})$, $t = 58.8$; (*c*) maximum $E(\frac{1}{2}\alpha_{\mathrm{KH}})$, $t = 76.1$; (*d*) local minimum $E(\frac{1}{2}\alpha_{\mathrm{KH}})$, $t = 89.9$; (*e*) local maximum $E(\frac{1}{2}\alpha_{\mathrm{KH}})$, $t = 104$; (*f*) local minimum $E(\frac{1}{2}\alpha_{\mathrm{KH}})$, $t = 128$. The domain length is $L = 2\lambda_{\mathrm{KH}}$ and contour intervals remains fixed throughout the wave history. The fields shown here correspond to the simulation of figure 12(*b*).

tion of the higher temporal frequency into the energy cycle as well as the initial substantial increase in wave kinetic energy.

Figure 19 shows that subharmonic growth is curtailed when the mean flow kinetic energy is diverted from the subharmonic into the potential energy $\bar{P}$ and, to a lesser extent, the kinetic energy of the fundamental component $E(\alpha_{\mathrm{KH}})$. Figure 18 shows that this increase in $\bar{P}$ is associated with a substantial increase in wave height, as the billow expends kinetic energy in order to raise heavier fluid into the upper (less dense) stream and force lighter fluid into the lower (more dense) stream. The maximum wave height clearly occurs in figure 18(*d*) which most closely corresponds to the state of maximum potential energy $\bar{P}$. This latter state lags the state of maximum subharmonic kinetic energy (figure 18*c*) by a substantial time interval.

During the next phase of flow evolution, the potential energy and the subharmonic

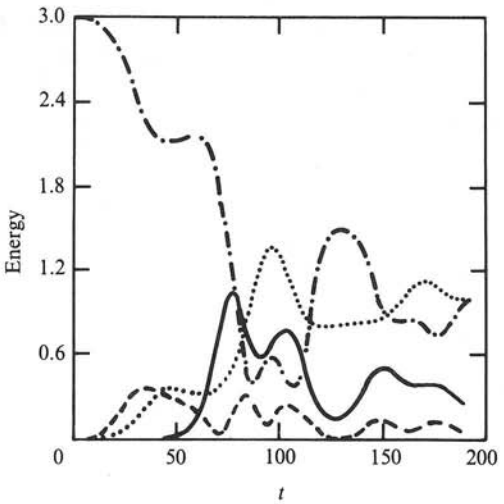

FIGURE 19. Evolution of kinetic energies associated with the mean (–·–, $E(0)$), subharmonic (——, $E(\frac{1}{2}\alpha_{\mathrm{KH}})$), and fundamental (– – –, $E(\alpha_{\mathrm{KH}})$), components of the pairing simulation shown in figures 18 and 12(*b*). Evolution of the potential energy $\bar{P}$(· · · · ·) is also shown. Note that for purposes of clarity $E(0)$ has been reduced by an amount $E_0 = 4.9$ and the value of $\bar{P}$ has been increased so that $\bar{P}(t = 0) = 0$.

kinetic energy both decrease as energy is returned to the mean shear flow. The fluid that has been forced into the high-speed streams during the period of active wave growth is drawn out into thin nearly horizontal layers. As a measure of how drastically this process depletes the billow, the wave kinetic energy $K \approx E(\frac{1}{2}\alpha_{\mathrm{KH}})$ at $t = 128$ (corresponding to maximum $E(0)$) is only about half the maximum kinetic energy achieved by the fundamental mode at $t = 34.6$. This reinforcement of the mean shear sets the stage for renewed wave growth at $t \gtrsim 130$.

It is well known that further amalgamations may take place after the initial pairing event is complete. For example Corcos & Sherman (1984) have numerically traced the evolution of an unstratified shear layer through two successive pairing events. Winant & Browand (1974) have observed four sequential pairings in a homogeneous shear layer, the limit being imposed by the upper and lower boundaries of the apparatus. However, Koop & Browand (1979) have observed that the pairing process is inhibited by stable stratification. For the value of stratification considered in the present work ($Ri = 0.07$), Koop & Browand report that the majority of vortices experience only a single pairing. Furthermore, we have shown that pairing in stratified flow can be substantially delayed if the subharmonic amplitude is low or if its horizontal phase is misaligned at the time nonlinear effects become important. Thus, the effects of the energy cycle oscillations that occur in our stratified simulations with $L = \lambda_{\mathrm{KH}}$ and $L = 2\lambda_{\mathrm{KH}}$ are expected to be observable in unforced shear layers. Indeed the tilting of the major axes of the billow cores, a behaviour associated with the energy cycle, is clearly evident in the observational data presented by Hernan & Jimenez (1982).

Figure 20 displays the shear layer evolution for a simulation in which the model domain length is set to $3\lambda_{\mathrm{KH}}$ and the initial long-wave perturbation (i.e. wavelength $3\lambda_{\mathrm{KH}}$) is in phase with the fundamental disturbance. In this configuration of the numerical model, the first subharmonic of the fundamental KH mode is excluded from the Fourier spectrum of the shear layer. Thus pairing instability is impossible

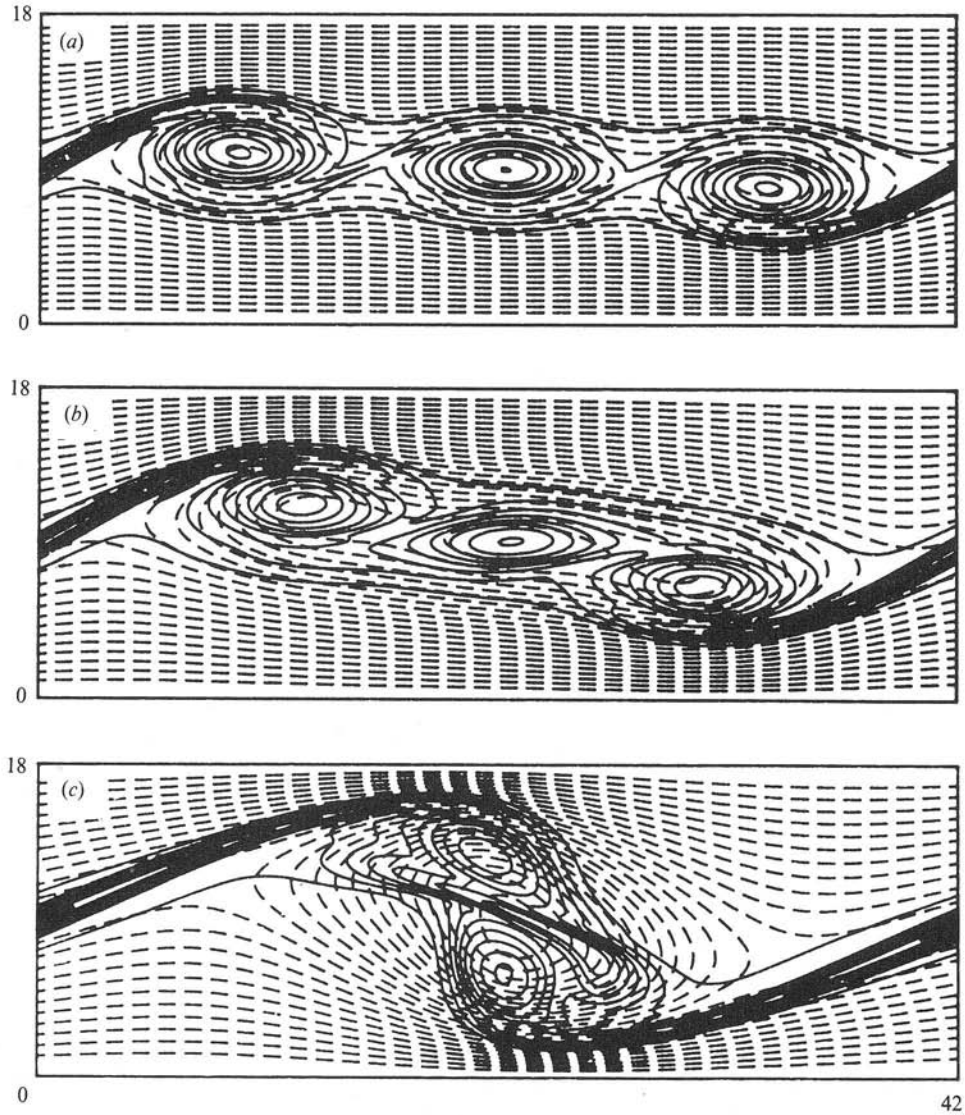

FIGURE 20. Evolution of the vorticity field in a $3 \rightarrow 1$ event. Since the domain length $L = 3\lambda_{KH}$, the components responsible for pairing are excluded from the simulation. The model is initialized with the incipient long-wave core centred at $x = \frac{3}{2}\lambda_{KH}$. Non-dimensional times are (*a*) $t = 62.3$, (*b*) 76.1, and (*c*) 89.9.

and vortex amalgamation may proceed through tripling interaction. Figure 20 demonstrates that one of the possible tripling interactions consists of the simultaneous amalgamation of three vortices. In the early nonlinear stages of the tripling interaction, the left-most vortex is raised above the centre of the shear layer and the rightmost vortex is forced below it, so that the three vortex centres approximately define a line having negative slope. Orbital motion of this kind, which is in the same sense as the rotation associated with the mean flow, is similar to that observed in the pairing process.

When the phase of the perturbation with wavelength $3\lambda_{KH}$ is shifted by $\frac{1}{2}\pi$ radians relative to the fundamental, a rather different outcome is observed (see figure 21).

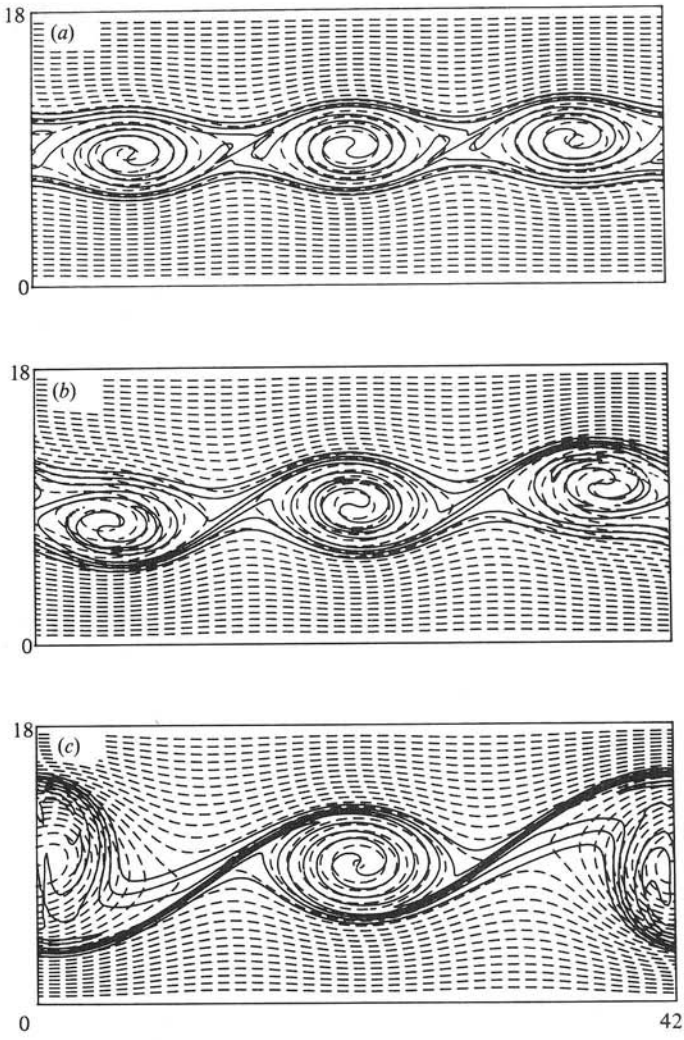

FIGURE 21. Evolution of the potential temperature field in a $3 \rightarrow 2$ event. This simulation is initialized with the incipient long-wave core centred at $x = 0$. (Pairing is excluded by the choice of domain length.) Non-dimensional times are (*a*) $t = 62.3$, (*b*) 76.1, and (*c*) 89.9.

The phase of the long wave in this case favours a tripling interaction in which three vortices combine to form two. In the early nonlinear stages, the leftmost vortex is forced below the centre of the shear layer, while the rightmost is lifted above it, so that the three vortices approximately define a line having positive slope. This motion has a rotational sense about the point $z = \frac{1}{2}H$, $x = \frac{3}{2}\lambda_{\mathrm{KH}}$ that is opposite to that required for orbital merging, so that a $3 \rightarrow 1$ interaction cannot occur. However the rotational sense of the displacement about the point $z = \frac{1}{2}H$, $x = 0$ (or $x = L$) is consistent with orbital amalgamation of the leftmost and rightmost vortices (recall that the horizontal domain is periodic), so it is not surprising that these two vortices merge. It should be emphasized that this $3 \rightarrow 2$ interaction is not a process in which two vortices merge and leave the third unaffected – the wavelengths of the two vortices shown in figure 21 (*c*) are $1.8\lambda_{\mathrm{KH}}$ and $1.2\lambda_{\mathrm{KH}}$ (giving a mean wavelength of $1.5\lambda_{\mathrm{KH}}$ for the layer, which is consistent with a $3 \rightarrow 2$ interaction). Also, the

amplitude of the lone vortex is increased by this interaction, indicating that the two merging vortices also transfer some of their kinetic energy to it. Upon completion of a $3 \rightarrow 2$ orbital amalgamation, the component $k = \frac{2}{3}\alpha_{KH}$ contains the major portion of the wave kinetic energy, whereas the $3 \rightarrow 1$ interaction leads to the dominance of the $k = \frac{1}{3}\alpha_{KH}$ component.

The simulations shown in figures 20 and 21 indicate that a variety of complex subharmonic merging interactions may occur in a free shear layer. The tripling interactions we have demonstrated are completed before deformational merging can be excited (see figure 10) and thus unambiguously represent realizations of orbital merging. They confirm our interpretation given in §§5 and 6 that orbital merging instability with $b = \frac{1}{3}\alpha_{KH}$ can correspond to either a $3 \rightarrow 1$ or a $3 \rightarrow 2$ interaction, depending on which of the two dominant components of the eigenfunction is most strongly amplified. Our preliminary results suggest that it is the relative phase of the $k = \frac{1}{3}\alpha_{KH}$ and $k = \frac{2}{3}\alpha_{KH}$ components with respect to the fundamental that determines the outcome of the interaction.

It is most instructive to review these vortex merging processes in the context of data reported by Hernan & Jimenez (1982) for the unstratified mixing layer. Their figure 9 shows a continuous distribution of eddy wavelengths in the mixing layer, a feature consistent with the finite bandwidth of the primary KH and secondary amalgamation instabilities. If pairing were the sole process acting to increase the predominant wavelength in the layer, one would expect to see peaks at $\lambda = 2n\lambda_{KH}$, where $n = 0, 1, 2, \ldots$. However peaks in the observed spectrum occur at $\lambda = \lambda_{KH}$, $1.5\lambda_{KH}$, $2\lambda_{KH}$, $3\lambda_{KH}$ and $4\lambda_{KH}$. The peak at λ_{KH} is due to KH instability. The fact that the bandwidth of the peak is much narrower than the bandwidth predicted by a linear stability analysis of the parallel flow may be attributed to nonlinear effects. Pairing instability clearly contributes to the peak at $2\lambda_{KH}$. Since the layer in the experiments under consideration is unstratified, vortex-draining instability also appears to contribute. Hernan & Jimenez have identified a somewhat infrequent 'bleeding' interaction (at the 10% occurrence level) in which an eddy stopped growing and was slowly absorbed by its neighbours. The rather minor peak at $4\lambda_{KH}$ is evidently a consequence of double pairings and perhaps even quadrupling interactions.

The intermediate peak at $3\lambda_{KH}$ has been attributed by Hernan & Jimenez to a two-stage amalgamation process in which 'an eddy of size one, when paired with a previously doubled eddy of size two, will give something of size roughly equal to three'. Although a two-stage process of the kind proposed by Hernan & Jimenez is a possible contributing factor to this peak, our stability analyses together with the simulation of figure 20 provide a more direct mechanism for generating vortices of this length from KH billows, namely the excitation of $3 \rightarrow 1$ merging instability with $b = \frac{1}{3}\alpha_{KH}$ (vortex tripling). Our simulation shown in figure 21 also provides a mechanism for generating waves of average length $1.5\lambda_{KH}$, namely the excitation of a $3 \rightarrow 2$ merging instability with Floquet parameter $b = \frac{1}{3}\alpha_{KH}$. (Note that this $1.5\lambda_{KH}$ peak corresponds to the highest frequency of occurrence in the layer.) Hernan & Jimenez have reported that tripling processes comprise 10% of the vortex interactions observed in an unstratified mixing layer in the absence of forcing.

Ho & Huang (1982) have used weak forcing to excite various vortex merging interactions in mixing-layer experiments. When the forcing has a wavelength λ_f such that $\lambda_f \lesssim 2\lambda_{KH}$ the observed response has wavelength λ_f, and vortex merging is suppressed relative to the case in which subharmonic forcing is present. These data illustrate the dramatic effect that the initial relative amplitude of the subharmonic

and fundamental has on the onset of pairing instability. When the layer is forced in the range $3\lambda_{KH} \lesssim \lambda_f \lesssim 4\lambda_{KH}$, vortices merge in groups of three. The merging pattern most often observed in this case was a $3 \rightarrow 2$ interaction, although altering the phase of the forcing enhanced the occurrence of $3 \rightarrow 1$ events. This phase-displacement effect is consistent with the phase relationship we have found between the $3 \rightarrow 2$ and $3 \rightarrow 1$ orbital merging interactions.

8. Discussion

Our stability analyses of Stuart and Kelvin–Helmholtz vortices have demonstrated the existence of two distinct types of amalgamation instability, namely orbital and deformational merging, and that both are supercritical Hopf bifurcations. The first subharmonic in the orbital branch corresponds to the familiar pairing instability, while the same mode in the deformational branch corresponds to vortex-draining instability.

Theoretical analyses of orbital-merging instability date back to the work of von Kármán (see Lamb 1932), who employed the Biot–Savart law to show that a row of like-signed point vortices was unstable with respect to a continuous spectrum of modes, and that the most unstable of these corresponded to the first subharmonic of the row wavenumber. His prediction of $\sigma = \alpha(1-\alpha)$ for the dependence of the growth rate on the disturbance wavenumber α (given in units of the row wavenumber) agrees very closely with our calculation of the stability of a row of Stuart vortices in the point-vortex limit $A \rightarrow 1$.

Kelly (1967) considered the stability of more realistic continuous vorticity distributions, employing a weakly nonlinear method to make the analysis more tractable. Vortex merging was conceptualized as a resonant feedback process in which a pair of waves mutually reinforced each other through interactions with the primary vortex, thereby enhancing their growth with respect to the rate arising from instability of the parallel flow alone. When this theory was employed to calculate the stability of Stuart vortices in the limit $A \rightarrow 0$, enhanced growth was found to be restricted to a rather narrow band of wavenumbers, centred on the first subharmonic and estimated to be of order-A width.

The calculations reported in the present study show that the bandwidth of Stuart vortex-merging instability is of order-1 for amplitudes as small as $A = 0.01$. (Note that Kelly had expected the resonance theory to be valid for periodic disturbances with amplitudes up to $A = 0.1$ or 0.2.) An examination of the structure of the vortex merging eigenfunctions calculated with our general theory shows that the dominant components have horizontal wavenumbers given by $k = b$ and $k = b - \alpha_s$, where $b < \alpha_s$, and α_s is the Stuart vortex wavenumber. The fact that the resonance theory did not include the latter component could explain the bandwidth discrepancy we have found. Our calculations also yield a subharmonic growth rate versus amplitude dependence ($d\sigma/dA = 0.50$) that differs from the resonance theory value by roughly a factor of two. (According to Kelly (1967, p. 661), our Stuart vortex amplitude A corresponds to his $(C^2-1)^{\frac{1}{2}}/C \approx \delta - \frac{1}{2}\delta^3 + \ldots$. Thus in the limit of small δ, our A corresponds to Kelly's δ and the total horizontal velocity field of the Stuart vortex is given by

$$\frac{\partial \psi}{\partial y} = \tanh y + \delta \operatorname{sech} y \tanh y \cos x.$$

An anonymous referee has pointed out that Kelly may have used $2\delta \operatorname{sech} y \tanh y \cos x$ for the Stuart vortex perturbation velocity, and, if this is the case, Kelly's reported pairing instability growth rate should have been 0.4824δ rather than 0.9648δ.)

Kelly's theory has recently been extended to the case in which the horizontal phase of the subharmonic relative to the periodic flow is allowed to vary continuously (see Ho & Huerre 1984). The modified growth rate was found to vary smoothly from a maximum when the fundamental and subharmonic were in phase to a minimum when they were directly out of phase. Although this latter behaviour could be considered as somewhat suggestive of the differences between vortex pairing and draining instabilities, it should be emphasized that our theory has demonstrated that pairing and draining constitute two distinct forms of vortex merging, and that each has a unique value of the relative horizontal phase.

The analyses presented here have shown that vortex pairing is the most rapidly amplified mode in a rather broad continuous spectrum of orbital vortex merging instabilities. Consequently it is this first subharmonic component that is most likely to impose its wavelength on the layer. However, minor variations in the initial spectrum of noise can lead to the dominance of other wavelengths close to the first subharmonic. Furthermore, the bandwidth of merging instability is sufficiently broad for a relatively modest bias in the initial conditions to lead to the collective merging of three or perhaps even four vortices in a single interaction. (The second subharmonic growth rate is only 12 % lower than that of the first.) The predictions of our theory are supported by experimental data that show that vortex tripling interactions occur at the 10 % frequency level in an unforced homogeneous mixing layer (Hernan & Jimenez 1982), and tripling events can constitute the dominant vortex amalgamation process in an appropriately forced shear layer (Ho & Huang 1982).

Nonlinear simulations with a horizontal model domain equal to three times the wavelength of the fundamental KH billow have demonstrated that the relative horizontal phase of the second subharmonic and the fundamental components at the time nonlinear effects commence determines the outcome of the tripling interaction, i.e. either a $3 \rightarrow 2$ or a $3 \rightarrow 1$ orbital amalgamation may occur. This result is consistent with the behaviour observed in forced-mixing-layer experiments by Ho & Huang (1982) and provides an explanation for the peaks found at $1.5\lambda_{KH}$ and $3\lambda_{KH}$ in the unforced-mixing-layer experiments of Hernan & Jimenez (1982).

Our calculations indicate that vortex-draining instability is similar to an interaction observed in unstratified free shear layers by Hernan & Jimenez (1982), in which vortices 'disintegrate slowly while they are bled by their neighbours'. Nonlinear numerical simulations by Riley & Metcalfe (1980) indicate that it is possible to excite vortex draining interactions in unstratified free shear layers by altering the relative initial phase of the fundamental and the subharmonic. However, our nonlinear simulations indicate that in a moderately stratified ($Ri = 0.07$) unforced shear layer, orbital merging is the most probable amalgamation process for any combination of initial phases. Thus it appears that vortex-draining instability may only be of significance in unstratified or weakly stratified flow.

Our analyses indicate that another type of transverse instability, which leads to a temporary distortion of the braids joining neighbouring billows, can occur in moderately stratified KH flow. This instability presents a plausible explanation of the wave-like disturbances observed to form on the braids of KH billow in naturally occurring flows (e.g. Thorpe 1968; Woods 1969). Since the braid distortions are evidently not due to secondary KH instability there is no compelling reason to believe that the mechanism causing them should necessarily have transverse symmetry. In future work we intend to examine the three-dimensional character of this instability. If the fastest-growing mode does have a non-zero spanwise wavenumber, it would in principle be possible for the braid instability to play a role

in the onset of small-scale disorder. We also note that our nonlinear simulations have demonstrated that secondary KH instability can occur *after* vortex pairing is completed.

Of the instabilities considered here, the two that appear to have the greatest potential impact on the long-term evolution of the shear layer are the transverse vortex pairing and longitudinal instabilities (the latter being translative for unstratified flow and convective for stratified flow). The question of which instability dominates is an important one and is a subject of current research on which we will report in due course.

The computations were carried out on the Cray supercomputers at the Centre Informatique de Dorval and the Ontario Centre for Large Scale Computation. This research was supported through grants from the Natural Sciences and Engineering Research Council and the Atmospheric Environment Service of Canada.

REFERENCES

Bernal, L. P., Breidenthal, R. E., Brown, G. L., Konrad, J. H. & Roshko, A. 1980 On the development of three-dimensional small scales in turbulent mixing layers. In *Turbulent Shear Flows 2* (ed. L. J. S. Bradbury, F. Durst, B. E. Launder, F. W. Schmidt & J. H. Whitelaw), p. 305. Springer.

Bernal, L. P. & Roshko, A. 1986 Streamwise vortex structure in plane mixing layers. *J. Fluid Mech.* **170**, 499–525.

Breidenthal, R. E. 1981 Structure in turbulent mixing layers and wakes using a chemical reaction. *J. Fluid Mech.* **109**, 1–24.

Browand, F. K. 1966 An experimental investigation of the instability of an incompressible separated shear layer. *J. Fluid Mech.* **26**, 281–307.

Browand, F. K. & Winant, C. D. 1973 Laboratory observations of shear-layer instability in a stratified fluid. *Boundary-Layer Met.* **5**, 67–77.

Corcos, G. M. & Lin, J. S. 1984 The mixing layer: deterministic models of a turbulent flow. Part 2. The origin of the three-dimensional motion. *J. Fluid Mech.* **139**, 67–95.

Corcos, G. M. & Sherman, F. S. 1976 Vorticity concentration and the dynamics of unstable free shear layers. *J. Fluid Mech.* **73**, 241–264.

Corcos, G. M. & Sherman, F. S. 1984 The mixing layer: deterministic models of a turbulent flow. Part 1. Introduction and the two-dimensional flow. *J. Fluid Mech.* **139**, 29–65.

Craik, A. D. D. & Criminale, W. O. 1986 Evolution of wavelike disturbances in shear flows: a class of exact solutions of the Navier–Stokes equations. *Proc. R. Soc. Lond.* A **406**, 13–26.

Davis, P. A. & Peltier, W. R. 1979 Some characteristics of the Kelvin–Helmholtz and resonant overreflection modes of shear flow instability and of their interaction through vortex pairing. *J. Atmos. Sci.* **36**, 2395.

Freymuth, P. 1966 On transition in a separated laminar boundary layer. *J. Fluid Mech.* **25**, 683–704.

Hernan, M. A. & Jimenez, J. 1982 Computer analysis of a high speed film of the plane turbulent mixing layer. *J. Fluid Mech.* **119**, 323–345.

Ho, C.-M. & Huang, L. S. 1982 Subharmonics and vortex merging in mixing layers. *J. Fluid Mech.* **119**, 443–473.

Ho., C.-M. & Huerre, P. 1984 Perturbed free shear layers. *Ann. Rev. Fluid Mech.* **16**, 365–424.

Jimenez, J., Cogollos, M. & Bernal, L. P. 1985 A perspective view of the plane mixing layer. *J. Fluid Mech.* **152**, 125–143.

Kelly, R. E. 1967 On the stability of an inviscid shear layer which is periodic in space and time. *J. Fluid Mech.* **27**, 657–689.

Klaassen, G. P. & Peltier, W. R. 1985*a* The evolution of finite amplitude Kelvin–Helmholtz billows in two spatial dimensions. *J. Atmos. Sci.* **42**, 1321–1339.

Klaassen, G. P. & Peltier, W. R. 1985*b* The onset of turbulence in finite-amplitude Kelvin–Helmholtz billows. *J. Fluid Mech.* **155**, 1–35.

Klaassen, G. P. & Peltier, W. R. 1985*c* The effect of Prandtl number on the evolution and stability of finite amplitude Kelvin–Helmholtz billows. *Geophys. Astrophys. Fluid Dyn.* **32**, 23–60.

Klaassen, G. P. & Peltier, W. R. 1987 Secondary instability and transition in finite amplitude Kelvin–Helmholtz billows. In *Proc. Third Intl Symp. on Stratified Flows, 3–5 Feb. 1987. Pasadena, California*, Vol. I (ed. E. J. List & G. Jirka).

Koop, C. G. & Browand, F. K. 1979 Instability and turbulence in a stratified fluid with shear. *J. Fluid Mech.* **93**, 135–159.

Lamb, H. 1932 *Hydrodynamics*, 6th edn. Dover.

Lasheras, J. C. & Choi, H. 1988 Three-dimensional instability of a plane, free shear layer: an experimental study of the formation and evolution of streamwise vortices. *J. Fluid Mech.* **189**, 53–86.

Maslowe, S. A. 1973 Finite amplitude Kelvin–Helmholtz billows. *Boundary-Layer Met.* **5**, 43–52.

Miksad, R. W. 1972 Experiments on the nonlinear stages of free-shear-layer transitions. *J. Fluid Mech.* **56**, 695–719.

Nagata, M. & Busse, F. H. 1983 Three-dimensional tertiary motions in a plane shear layer. *J. Fluid Mech.* **135**, 1–26.

Patnaik, P. C., Sherman, F. S. & Corcos, G. M. 1976 A numerical simulation of Kelvin–Helmholtz waves of finite amplitude. *J. Fluid Mech.* **73**, 215–240.

Peltier, W. R., Hallé, J. & Clark, T. L. 1978 The evolution of finite amplitude Kelvin–Helmholtz billows. *Geophys. Astrophys. Fluid Dyn.* **10**, 53–87.

Pierrehumbert, R. T. & Widnall, S. E. 1982 The two- and three-dimensional instabilities of a spatially periodic shear layer. *J. Fluid Mech.* **114**, 59–82.

Riley, J. J. & Metcalfe, R. W. 1980 Direct numerical simulation of a perturbed turbulent mixing layer. *AIAA Paper* 80-0274.

Stuart, J. T. 1967 On finite amplitude oscillations in laminar mixing layers. *J. Fluid Mech.* **29**, 417–440.

Thorpe, S. A. 1968 A method of producing a shear flow in a stratified fluid. *J. Fluid Mech.* **32**, 693–704.

Thorpe, S. A. 1973 Experiments on stability and turbulence in a stratified shear flow. *J. Fluid Mech.* **61**, 731–751.

Thorpe, S. A. 1985 Laboratory observations of secondary structures in Kelvin–Helmholtz billows and consequences for ocean mixing. *Geophys. Astrophys. Fluid Dyn.* **34**, 175–199.

Thorpe, S. A. 1987 Transition phenomena and the development of turbulence in stratified fluids. *J. Geophys. Res.* **92**, 5231.

Winant, C. D. & Browand, F. K. 1974 Vortex pairing: the mechanism of turbulent mixing layer growth at moderate Reynolds numbers. *J. Fluid Mech.* **63**, 237–255.

Woods, J. D. 1969 On Richardson's number as a criterion for laminar–turbulent–laminar transition in the ocean and atmosphere. *Radio Sci.* **4**, 1289–1298.